Nitrogen cycle in the Late Archean ferruginous ocean

Vincent Busigny, Oanez Lebeau, Magali Ader, Bryan Krapež, Andrey Bekker

Nitrogen cycle in the Late Archean ferruginous ocean

Vincent Busigny[1*], Oanez Lebeau[1], Magali Ader[1], Bryan Krapež[2], Andrey Bekker[3]

[1] *Institut de Physique du Globe de Paris, Sorbonne Paris Cité, Univ. Paris Diderot, UMR 7154 CNRS, 1 rue Jussieu, 75238 Paris, France*

[2] *The Institute for Geoscience Research, Department of Applied Geology, Curtin University, GPO Box U1987, Perth WA 6845, Australia*

[3] *Department of Geological Sciences, University of Manitoba, 125 Dysart Road (Wallace Building), Winnipeg, Manitoba, R3T 2N2, Canada*

[*]Corresponding author. *E-mail address:* busigny@ipgp.fr

Submitted to Chemical Geology "Dick Holland special volume"

Abstract

The Hamersley Group comprises a Late Archean sedimentary succession, which is thought to record the prelude to the atmospheric oxygenation in the Paleoproterozoic, the so-called Great Oxidation Event (GOE), at ~2.4 Ga. We studied drill-core samples of sedimentary rocks from the upper Mount McRae Shale and Brockman Iron Formation deposited before the GOE at ~2.5 Ga in order to characterize the environments and ecosystems prevailing during their deposition. The rocks from the Mount McRae Shale and Brockman Iron Formation represent, respectively, proximal euxinic conditions and distal ferruginous depositional environments, thus providing an opportunity to examine lateral variability in the open-marine basin. We analyzed the concentration and isotopic composition of carbon in carbonate and organic matter, bulk nitrogen content and its isotopic composition as well as major element concentrations. The $\delta^{13}C_{carb}$ values and carbonate content range from -3.2 to -10.7 ‰ and 0.1 to 58 wt%, respectively. Organic carbon content also varies over a large range from 0.05 to 4.6 wt% with a near constant $\delta^{13}C_{org}$ value of -28.7 ± 0.8 ‰. Negative $\delta^{13}C_{org}$ excursions (down to -31 ‰) are generally correlated with high organic matter content. Bulk nitrogen shows highly variable concentration, between 1.3 and 785 ppm, and $\delta^{15}N$ values between 0.4 and 13.4 ‰.

The $\delta^{13}C_{carb}$ values reflect a diagenetic carbonate origin, with negative values typical for Fe-rich carbonates formed by organic matter mineralization with ferric oxyhydroxides. In contrast, $\delta^{13}C_{org}$ and $\delta^{15}N$ values record primary isotope signatures derived from ancient living organisms. The relatively constant $\delta^{13}C_{org}$ values at around -28.7 ‰ are interpreted as reflecting photoautotrophs utilizing a large pool of dissolved inorganic carbon. Inverse stratigraphic co-variation between $\delta^{15}N$ and $\delta^{13}C_{carb}$ values was observed for the Brockman Iron Formation. We

propose that N and C biogeochemical cycles were coupled by Fe redox cycling in the water column and in sediments of the Late Archean ocean. Several models for biogeochemical N cycling linked to the redox structure of the water column are considered. Under fully anoxic conditions, the dominant N species available for assimilation by micro-organisms in the photic zone could be ammonium (NH_4^+). Highly positive $\delta^{15}N$ values would reflect the assimilation of NH_4^+ enriched in ^{15}N by partial oxidation to nitrite, followed by quantitative removal of the produced nitrite by denitrification or anamox processes. Ammonium oxidation could have been driven by (i) O_2 produced locally via oxygenic photosynthesis, or (ii) microbial oxidation utilizing Fe(III)-oxyhydroxides formed in the water column. Under redox-stratified conditions, N assimilated by primary producers could have been in the form of NO_3^-, based on modern and Phanerozoic analogues. The positive $\delta^{15}N$ values would have resulted in this case from partial denitrification of NO_3^- coupled to anaerobic microbial oxidation of Fe(II) to Fe(III). We conclude that similar positive $\delta^{15}N$ signatures may record very different N biogeochemical cycles under anoxic, stratified and fully oxic conditions in the ocean. Interpretation of the N isotopes in terms of N biogeochemical cycle thus requires independent constraints on the redox structure of the ocean.

Keywords: nitrogen; carbon; isotopes; Archean ocean; banded iron formation

1. Introduction

One of the most important changes in Earth's surface history is the oxygenation of the atmosphere-ocean system (Holland, 1984, 2009). The oxygenation imparted major modifications to the geochemical cycles of many redox-sensitive elements, such as C, O, N, S, and base metals, with dramatic implications for the development and evolution of life (Anbar and Knoll, 2002). It is now well established that the first irreversible oxygenation of the atmosphere, the so called Great Oxidation Event (GOE), occurred between 2.4 and 2.3 Ga (Holland, 2002; Bekker et al., 2004; Guo et al. 2009), although transient oxygenation could have occurred earlier. Recent studies of the Mount McRae Shale, Western Australia suggested that atmospheric oxygenation started at 2.5 Ga, based on Mo and Re concentrations and isotopic compositions (Anbar et al., 2007), and C and S isotope values of whole-rock shale samples (Kaufman et al., 2007). Nitrogen isotope (Garvin et al., 2009) and Fe speciation (Reinhard et al., 2009; Raiswell et al., 2011) studies of the same sample set also argued for surface ocean oxygenation at that time. Earlier oxygenation of the surface ocean at ~2.67 Ga was proposed based on N isotope composition of shales from the Campbellrand-Malmani carbonate platform, South Africa (Godfrey and Falkowski, 2009). Besides the question of timing, the secular trend of O_2 accumulation in the atmosphere-ocean system is also highly debated. Two secular trends have been proposed: (1) gradual O_2 increase and accumulation (e.g., Holland, 2006; Murakami et al., 2011), and (2) oscillatory variations in O_2 level in association with the early Paleoproterozoic glacial events and the Lomagundi carbon isotope excursion (Bekker and Kaufman, 2007; Bekker and Holland, 2012). The Late Archean may also have been characterized by transient and local low-levels of oxygen, so-called "whiffs" of oxygen (Anbar et al., 2007).

Nitrogen isotopes represent a unique tool for exploring the secular evolution of oxygen because (i) N biogeochemistry is mainly controlled by redox reactions and (ii) N is present in all sedimentary rocks, providing a continuous record in different geological settings. In contrast to the Archean, the modern N cycle in the ocean is relatively well understood (see reviews in Brandes et al., 2007; Sigman et al., 2009). The main reservoir of N at the Earth's surface is the atmosphere with a present $\delta^{15}N$ value of 0 ‰ (N isotope composition is expressed as $\delta^{15}N = [(^{15}N/^{14}N)_{sample}/(^{15}N/^{14}N)_{standard} - 1] \times 1000$, where the standard is atmospheric N_2). Nitrogen enters the oceanic cycle through atmospheric N_2 fixation by aerobic and anaerobic autotrophs with minor N isotope fractionation (<3 ‰; e.g., Wada et al., 1975; Minagawa and Wada, 1986). After the death of these autotrophic organisms, organic matter mineralization releases N as ammonium (NH_4^+), with very little isotopic fractionation (Prokopenko et al., 2006; Möbius, 2013). In the presence of free O_2, NH_4^+ is oxidized into nitrate (NO_3^-) during a two-step biological process called nitrification, which is associated with significant N isotope fractionation ~16 ‰ (Sigman et al., 2009). This fractionation is rarely fully expressed in modern marine environments since the transformation of NH_4^+ to NO_3^- is generally complete. In O_2-depleted environments such as oxygen-minimum zones or anoxic sediments, nitrates are partially reduced by denitrification or anammox (i.e., anaerobic ammonium oxidation) into gaseous N_2 or N_2O. During denitrification, ^{14}N is preferentially released relative to ^{15}N, leaving residual marine NO_3^- enriched in the heavy isotope (average marine $\delta^{15}N_{NO3-} \sim +5$ ‰; e.g., Altabet and François, 1994). The heavy isotope signature of NO_3^- is transferred by assimilation to organisms living in the water column or in the diagenetic realm and then recorded in sedimentary organic matter. Accordingly, assuming a steady-state system, the N isotope composition of organic matter in modern marine environment reflects mainly the relative proportion of N denitrification (in the water column and in sediments)

and N fixation. In O_2-free environments such as the Early Archean oceans, the nitrification and thus subsequent denitrification are unlikely, and dissolved N species may have been dominated by NH_4^+ (Holland, 1984, 2002; Beaumont and Robert, 1999; Papineau et al., 2005). Accordingly, N cycle and isotope composition of Archean ocean and sediments may have been significantly different from those of the modern world (Canfield et al., 2010).

Most of the N in the Earth exosphere is contained as N_2 in the atmosphere (presently ~ 3.98×10^{21} g). Based on data from fluid inclusion in cherts (Sano and Pillinger, 1990) and geochemical modeling (Tolstikhin and Marty, 1998), the N isotope composition of the atmosphere is believed to have remained largely constant during the last 3 Ga with $\delta^{15}N$ values of about 0‰. The use of N isotope compositions of Precambrian sedimentary rocks as a tracer of NO_3^-, and thus O_2, content was proposed in the pioneering work of Beaumont and Robert (1999). In their study, the authors analyzed cherts of various ages and suggested a dramatic change in the N biogeochemical cycle between 3 and 2 Ga. Negative $\delta^{15}N$ values were observed in cherts older than ~2.4 Ga and interpreted as reflecting N_2 fixation or NH_4^+ assimilation (Beaumont and Robert, 1999; Papineau et al., 2005), a result compatible with low NO_3^- concentrations (if any) under anoxic conditions in the early Earth oceans. However, this interpretation was questioned since some of these cherts were deposited in hydrothermal settings and may have recorded N isotope signatures of chemoautotrophic organisms specific to these environments (Pinti and Hashizume, 2001; Pinti et al., 2001, 2009). If this was the case, their N isotope signature would not reflect phototrophic organisms living in the photic zone of the upper ocean and the N isotope composition of seawater nitrogen compounds. Two recent N-isotope studies of Archean sedimentary sequences from Western Australia and South Africa suggested earlier oxygenation of the Earth's surface ocean starting at 2.5 Ga (Garvin et al., 2009) and 2.67 Ga (Godfrey and

153 Falkowski, 2009), respectively. Both studies identified $\delta^{15}N$ shifts from near 0 ‰ to positive
154 values, up to 7.5 ‰, and interpreted these trends as evidence for coupled nitrification-
155 denitrification, pathways typical of a surface ocean containing free O_2. According to their
156 interpretations, denitrification had to be partial so that N isotope fractionation can be expressed.
157 Bulk rock N isotope analyses of ~2.72 Ga carbonates from the Tumbiana Formation, Western
158 Australia revealed extreme $\delta^{15}N$ values up to +50.4 ‰, possibly recording the onset of
159 nitrification coupled to consumption of its products (nitrite and nitrate) via biological
160 denitrification (Thomazo et al., 2011). Such extreme N isotope compositions could only be
161 expressed under oxygen-limited conditions so that partial nitrification would be associated with
162 complete denitrification (Thomazo et al., 2011). High $\delta^{15}N$ values, up to +20 ‰, were also
163 observed in ~2.7 Ga carbonaceous shales from the Western Abitibi Greenstone Belt (Canada) and
164 Penhalonga Formation (Botswana). These values were explained by an Archean ^{15}N-enriched
165 atmosphere resulted from secondary accretion of C1 chondrite-like material (Jia and Kerrich,
166 2004a, 2004b). However, discrete N isotope excursions in time seem more likely than a long-
167 term evolution in composition of the atmosphere since other datasets illustrate very small, if any,
168 N isotope variations in the atmosphere through time (e.g., Sano and Pillinger, 1990; Tolstikhin
169 and Marty, 1998; Marty et al., 2012).

170 Previous studies of N isotopes in Precambrian rocks either (1) focussed on samples of
171 different lithologies and ages from different areas (e.g., Beaumont and Robert, 1999; Papineau et
172 al. 2005, 2009; Pinti et al., 2001, 2009; Jia and Kerrich, 2004b), or (2) analyzed stratigraphic
173 sequences of organic-rich shales (i.e., Garvin et al., 2009; Godfrey and Falkowski, 2009) or
174 carbonates (Thomazo et al., 2011). However, no study has presented so far a stratigraphic dataset
175 for a drill-core section of banded iron formation, which is one of the common Archean

176 sedimentary rocks. In this work, we analyzed the N isotope composition of drill core samples of
177 organic carbon-poor and Fe-rich sediments from the Brockman Iron Formation, Western
178 Australia, one of the best preserved banded iron formations in the world (Trendall and Blockley,
179 1970). The unit contains the products of redox reactions, including Fe oxidation in the water
180 column either by oxygenic or anoxygenic photosynthesis (e.g., Cloud, 1973; Konhauser et al.,
181 2002; Kappler et al., 2005; see also review in Bekker et al., 2010). Systematic N isotope study of
182 banded iron formations has never been performed before since they contain only small amounts
183 of N, requiring high-sensitivity techniques based on static mass-spectrometry. The Brockman
184 Iron Formation was deposited immediately above the Mount McRae Shale, which was
185 extensively studied previously to constrain the redox state of the atmosphere-ocean system
186 (Anbar et al., 2007; Kaufman et al., 2007; Garvin et al., 2009; Reinhard et al., 2009; Raiswell et
187 al., 2011). Accordingly, we build on these previous studies and continue to explore the
188 Hamersley Group in order to constrain environmental changes for the time period between ~2.5
189 and 2.46 Ga. In addition, samples from the Brockman Iron Formation were also selected because
190 they contain stilpnomelane, an Fe-rich mica-like silicate that may have preserved N isotope
191 signatures since NH_4^+ commonly substitutes for K^+ in K-bearing minerals (e.g., Honma and
192 Itihara, 1981; Boyd et al., 2001; Busigny et al., 2003a; Papineau et al., 2005). We found that N
193 concentrations are significantly higher in stilpnomelane-rich shale samples associated with
194 banded iron formation than in previously analyzed banded iron formation and chert samples
195 (Pinti et al., 2001, 2007, 2009). Nitrogen isotope analyses of our samples from the Mount McRae
196 Shale and Brockman Iron Formation were coupled with C isotope analyses of organic matter and
197 carbonates and measurements of major element concentrations. Both elemental and isotopic data
198 are used to separate primary signatures from late diagenetic and metamorphic overprints. Finally,

199 our results are compared to existing data in the literature and previously proposed models in order
200 to further develop and test existing models for the N biogeochemical cycle and redox structure of
201 the early Earth oceans before the GOE.
202
203 **2. Geological setting and sample description**
204
205 The rocks analyzed in our study belong to the Late Archean to early Paleoproterozoic
206 Hamersley Group (Western Australia), and include samples from the Mount McRae Shale and
207 Brockman Iron Formation (Fig. 1). They are composed of laminated and well-preserved
208 sediments that accumulated in relatively deep-water, marine environments below the wave base
209 (Pickard et al., 2004; Kaufman et al., 2007). For the Mount McRae Shale, regional sequence
210 stratigraphic analysis indicates the presence of two depositional cycles; each sequence starts with
211 carbonate and siliciclastic turbidite and breccia and deepens upwards to either semi-pelagic shale
212 or banded iron formation (Krapež et al., 2003). Bulk shale analyses of Re-Os isotopes gave an
213 age of 2501 ± 8 Ma for the Mount McRae Shale (Anbar et al., 2007) consistent with a high-
214 precision SHRIMP ^{207}Pb-^{206}Pb zircon age of 2504 ± 5 Ma for a tuff layer in the same unit
215 (Rasmussen et al., 2005). The Mount McRae Shale contains large amounts of organic C and
216 pyrite, which are mainly accompanied by quartz, siderite, dolomite, ankerite/ferroan dolomite,
217 chlorite, mica, K-feldspar, albite and minnesotaite (Krapež et al., 2003; Pickard et al., 2004;
218 Raiswell et al., 2011). The upper part of the Mount McRae Shale, the Colonial Chert Member, is
219 transitional to the Brockman Iron Formation (Trendall and Blockley, 1970). The Brockman Iron
220 Formation is composed of four stratigraphic units in ascending order: Dales Gorge, Whaleback
221 Shale, Joffre, and Yandicoogina Shale members (Trendall and Blockley, 1970; Krapež et al.,

2003). Depositional ages of ~2.48 and 2.46 Ga have been established for the Dales Gorge Member and the Whaleback Shale Member, respectively, based on U-Pb SHRIMP analyses of zircons from tuffaceous layers (Trendall et al., 2004). The Brockman Iron Formation contains alternating hematite-magnetite-chert (BIF) and chert-carbonate-silicate (S) decimeter to meter thick macrobands (Trendall and Blockley, 1970; Krapež et al., 2003; Fig. 1). Macrobands are divided into mesobands (10 to 50 mm in thickness) and laminated microbands (0.2 to 2 mm thick), composed of Fe-oxides, Fe-silicates, Fe-carbonates and chert in variable proportions with minor amounts of pyrite and organic carbon. Banded iron formations of the Brockman Supersequence have long been considered as pure marine chemical precipitates but were recently proposed to reflect episodic density flows (Krapež et al., 2003; Pickard et al., 2004; Rasmussen et al., 2013). Whole-rock major and trace element analyses suggest two dominant sources for BIF and S macrobands, with a major hydrothermal influence and a mafic provenance for BIF and a strong influence of continental and submarine weathering for S macrobands (Krapež et al., 2003; Pickard et al., 2004; Pecoits et al., 2009).

In the present work, we selected 31 samples from the Rio Tinto Exploration drill-core WLT-10, collected at 22.73°S and 116.75°E, approximately 100 km WNW from Paraburdoo township close to the south-western margin of the preserved extent of the basin, at depths ranging from 124 to 387 m (Fig. 1; see Table 1 for description of the samples). The samples are uniformly distributed through the uppermost part of the Mount McRae Shale to the unit J3 of the Joffre Member, spanning a depositional period of ~40 Ma. The units have experienced only minimal deformation and mild metamorphism (from 100°C to <300°C; Becker and Clayton, 1976; Smith et al., 1982; Kaufman et al., 1990), and carry primary chemical and isotopic signatures. The samples represent different lithologies of the Mount McRae Shale and Brockman

245 Iron Formation, thus allowing global changes in C and N biogeochemical cycles to be
246 distinguished from local variations related to either diagenetic or source-rock effects.
247
248 **3. Analytical techniques**
249
250 For each drill-core sample, uniform layers of 0.5 to 2 cm thick were selected, cut and
251 powdered to <60 μm. Carbon and N isotope analyses together with major element analyses were
252 performed on the same homogeneous powders. For C isotope analysis of carbonates, 3.26 to
253 109.09 mg of rock powder was loaded in a vacutainer tube. The tube was then flushed with
254 helium. Rock powder was treated with 100% phosphoric acid at 80°C for 2 hours and then at
255 130°C for another 2 hours. This treatment secured complete dissolution of carbonate (McCrea,
256 1950). Calcite and dolomite are expected to react at 80°C, while ankerite and siderite react at
257 130°C (Rosenbaum and Sheppard, 1986). Tests on samples subsequently heated to 150°C
258 produced no detectable CO_2. For each temperature step, C isotope composition of CO_2 was
259 measured using a continuous-flow mass-spectrometer (AP-2003) operated with helium as a
260 carrier gas. The isotopic data are reported in conventional δ units (in per mil) with respect to the
261 V-PDB standard. Analytical error on $\delta^{13}C$ values is better than ±0.1 ‰. Carbonate content in
262 samples was estimated from the ion intensity of the CO_2 peak in the mass-spectrometer with a
263 precision better than ±10% (2σ). Two to four replicate analyses of each sample were performed
264 for $\delta^{13}C_{carb}$ measurements, but only the average values are presented herein.
265 Total organic C content (TOC) and its C isotope composition were determined on
266 carbonate-free samples. Carbonates from powdered samples were removed using 6N HCl at 80°C
267 for 2 hours. The residue of decarbonation was rinsed with milliQ water several times until it

reached neutral pH, centrifuged and dried for 2 days at 50°C. Mass balance was used to estimate the amount of removed carbonate. Aliquots of dried decarbonated samples (50 to 100 mg for the Brockman Iron Formation samples and <10mg for the Mount McRae Shale samples) were then loaded into quartz tubes together with CuO wires, sealed under vacuum and combusted at 950°C for 6 hr (Duma combustion; cf., Bekker et al., 2001, Ader et al., 2006, 2009; Thomazo et al., 2009a; Sansjofre et al., 2011). The produced CO_2 was purified on a vacuum line and quantified manometrically; TOC content reproducibility was better than ±0.3 wt%. Carbon isotope composition of the purified CO_2 was then measured on a Delta^{plus}XP mass-spectrometer with a precision better than ±0.1 ‰. Results are reported using the $\delta^{13}C$ notation in per mil relative to V-PDB.

The procedure used for measurement of nitrogen content and its isotopic composition in rocks has been thoroughly described in previously published papers (Busigny et al., 2005; Ader et al., 2006) and is only summarized herein. Nitrogen was extracted from samples by combustion in quartz tubes sealed under vacuum. Before sample combustion, the powders were degassed under vacuum at 300°C for 12hrs. This degassing temperature is different from that previously used (450°C; Busigny et al., 2005; Ader et al., 2006) and was preferred for two reasons: (1) the Mount McRae Shale and Brockman Iron Formation have experienced a maximum burial temperature of 300°C (Smith et al., 1982; Kaufman et al., 1990), and (2) stilpnomelane, a potential N-bearing mineral phase, starts to break down at 450°C (Miyano and Klein, 1989). Nitrogen generated by combustion was then separated from other volatiles (mainly H_2O and CO_2) using purified Cu, CuO, and CaO (Kendall and Grim, 1990). It was quantified as dinitrogen (N_2) with a capacitance manometer on ultra-high vacuum line and its isotope analysis was performed on a triple-collector static vacuum mass-spectrometer, allowing measurement of nanomole

quantities of N_2. Nitrogen isotope composition is expressed in the $\delta^{15}N$ notation in per mil relative to atmospheric N_2. The quantity of N contributed by the analytical blank is low (0.65 ± 0.30 nmol N_2) and its isotope composition is -3.7 ± 2.7 ‰ (2σ). The precisions for sample nitrogen content and its isotope composition are better than 8% and 0.5 ‰, respectively.

Whole-rock concentrations of major elements were measured using ICP-AES at the Service d'Analyse des Roches et des Mineraux (SARM) of the Centre de Recherches Petrographiques et Geochimiques (CRPG) of Vandoeuvre, France. Analytical precision for major element concentrations is available at http://helium.crpg.cnrs-nancy.fr/SARM/pages/roches.html and typically better than 10%.

4. Results

4.1. Major element concentrations linked to petrology

Correlations observed between some major elements (Fig. 2) supports the identification of lithologies established during drill-core sampling and petrographic study. This shows a diversity of chemical compositions between several mineralogical end-members. Positive correlation among Al_2O_3, SiO_2, and K_2O (Fig. 2a and 2b) indicates that these elements are contained in the same phases, mostly stilpnomelane, but also mica and K-feldspar. Only one sample (DGM307-6) shows strong enrichment in SiO_2 (73 wt%) with no associated enrichment in Al_2O_3 (0.2 wt%). This sample is identified as a chert based on petrography. For all samples, an inverse correlation between Fe_2O_3 and SiO_2 (Fig. 2c) indicates that Fe-silicates do not represent one of the dominant Fe-bearing phases, in contrast to Fe-oxides (hematite and magnetite) and Fe-carbonates (siderite

and ankerite). It should be noted that our samples from the Mount McRae Shale differ from those of the Brockman Iron Formation in containing dolomite as a dominant carbonate phase while Fe-rich carbonates were not found by electron microprobe analysis. In contrast to the relationship between Al_2O_3 and K_2O, the best-fit line for Al_2O_3 and SiO_2 does not pass through the origin on the graph (Fig. 2a). Indeed, SiO_2 is at 10 to 20 wt%, when Al_2O_3 concentration is close to 0 wt%. This observation, coupled with petrography, indicates that most of our samples contain quartz (chert). Samples from the Brockman Iron Formation are strongly enriched in Fe with Fe_{Total} (expressed as Fe_2O_3) concentrations ranging from 6.7 to 78.2 wt% and averaging 33.8 ± 15.5 wt% (n=26). This differs significantly from the Mount McRae Shale samples, which have Fe_{Total} concentrations between 2.3 and 6.2 wt% (average is 3.8 ± 1.6 wt%, n=5). This contrast is also reflected in Fe/Ti molar ratios (Fig. 3). Fe-enrichment of the Brockman Iron Formation likely reflects contemporaneous anoxic and ferruginous conditions in the deep ocean (cf., Bekker et al., 2010), while the depositional environment of some portions of the Mount McRae Shale has been interpreted as anoxic and sulfidic (e.g., Reinhard et al., 2009; Raiswell et al., 2011).

To conclude, samples from the Brockman Iron Formation are mostly composed of potassium- and aluminum-rich silicates, Fe-oxides, quartz and carbonates in variable proportions. According to mineralogy and major element composition, our samples were divided into five rock types: organic-rich shale from the Mount McRae Shale, and stilpnomelane-rich mudrock, banded iron formation and chert from the overlying Brockman Iron Formation. Stilpnomelane-rich mudrocks were furthermore subdivided based on their carbonate content into carbonate-rich (>10 wt%) and carbonate-poor (<10 wt%) varieties.

336 *4.2. Carbon content and its isotope composition*

337

338 Carbonates contained in samples from the Mount McRae Shale were completely extracted
339 at temperature below 80°C and no signal was detected at 130°C, confirming that they contain no
340 siderite. About half of our samples from the Brockman Iron Formation were fully decarbonated at
341 80°C, while the other half still contained carbonate, which was extracted at 130°C. This clearly
342 points to the presence of siderite in half of these samples (Rosenbaum and Sheppard, 1986).
343 However, for both extraction temperatures (80°C and 130°C), $\delta^{13}C_{carb}$ values are nearly identical
344 within ±0.5 ‰. Thus, only bulk carbonate content and average $\delta^{13}C_{carb}$ values will be considered in
345 the following discussion. For the Brockman Iron Formation, the bulk carbonate content varies
346 greatly from less than 0.1 up to 83 wt%. The range of carbonate content in the Mount McRae
347 Shale from 8 to 57 wt% is smaller but still significant. The $\delta^{13}C_{carb}$ values measured in samples
348 from the Brockman Iron Formation (-10.7 to -5.1 ‰) are lower than those measured in samples
349 from the Mount McRae Shale (-5.6 to -3.2 ‰). The chemostratigraphic profile of C isotope
350 composition in carbonates shows significant variations, with intervals of increasing and
351 decreasing $\delta^{13}C_{carb}$ values (Fig. 4).

352 Depth profiles of C_{org} content and $\delta^{13}C_{org}$ values within the core are shown on Fig. 4. Data
353 for the Mount McRae Shale from Garvin et al. (2009) are also plotted for comparison. A strong
354 contrast is noticeable between samples from the Mount McRae Shale and Brockman Iron
355 Formation. The Mount McRae Shale is enriched in organic C with concentrations ranging from
356 1.7 to 16.1 wt% (average = 5.7 ± 3.8 wt%, 1σ), while samples from the Brockman Iron
357 Formation contain between 0.05 and 1.9 wt% of C_{org} (average = 0.7 ± 0.5 wt%, 1σ). This contrast
358 is even more pronounced in C_{org} isotope values, which roughly show a bimodal distribution with

359 the sharp transition from the Mount McRae Shale to the Brockman Iron Formation (Fig. 4). The
360 Mount McRae Shale has markedly negative $\delta^{13}C_{org}$ values, averaging -37.6 ± 2.8 ‰ (1σ), in
361 contrast to the Brockman Iron Formation with a mean $\delta^{13}C_{org}$ value of -28.7 ± 0.8 ‰ (1σ). The
362 heaviest C isotope composition (-26.4 ‰) is found in the chert DGM307-6 of the Brockman Iron
363 Formation, and corresponds to the lowest C_{org} content (0.05 wt%). The organic carbon content of
364 our complete sample set shows an inverse trend with Fe/Ti molar ratio (Fig. 3a), indicating that
365 Fe enrichment is associated with organic C depletion. Organic carbon contents also roughly
366 correlate with $\delta^{13}C_{carb}$ values with the most negative $\delta^{13}C_{carb}$ values corresponding to the lowest C_{org}
367 contents (Fig. 5).
368
369 *4.3. Nitrogen content and isotope composition*
370
371 Depth profiles of N content and $\delta^{15}N$ values within the drill-core are shown in Fig. 4.
372 Nitrogen content shows a similar stratigraphic pattern to that of C_{org} content (Fig. 4). This is also
373 illustrated by the positive correlation between these parameters (Fig. 6a). Samples from the
374 Mount McRae Shale are enriched in N with concentrations ranging between 385 and 786 ppm
375 (average = 495 ± 169 ppm, 1σ). In contrast, samples from the Brockman Iron Formation are
376 characterized by significantly lower N contents from 1.3 to 186 ppm (average = 55 ± 50 ppm,
377 1σ). Like organic C, N content decreases with increasing Fe/Ti molar ratio, indicating that Fe
378 enrichment is associated with low N concentrations (Fig. 3b). C_{org}/N molar ratios for the Mount
379 McRae Shale vary from 45 to 127 (average = 70 ± 35, 1σ). On the average, they are lower
380 compared to samples from the Brockman Iron Formation (mostly between 19 and 895, the
381 average is 242 ± 200, 1σ). Only one sample of the Brockman Iron Formation shows an

exceptionally high C_{org}/N ratio of 2251 (sample DGM288-2, Table 3). This high value is geologically relevant and is not an analytical artefact from incomplete carbonate dissolution, since this sample shows a $\delta^{13}C_{org}$ value of -29‰, indistinguishable from other samples (even minor carbonate contamination would significantly increase the measured $\delta^{13}C$ value). The depth profile of N isotope composition shows large variations in $\delta^{15}N$ values. These variations are independent of rock lithology, with N isotope values of organic-rich shale, carbonate-rich and carbonate-poor stilpnomelane mudrock, banded iron formation and chert fitting to the broad trend (Fig. 4). The $\delta^{15}N$ values range from 4.4 to 5.7 ‰ for the Mount McRae Shale (average = 4.9 ± 0.6 ‰, 1σ) and from 0.4 to 13.4 ‰ for the Brockman Iron Formation (average = 7.5 ± 2.7 ‰, 1σ). Pinti et al. (2001) analyzed one banded iron formation sample, containing magnetite, quartz and chlorite, from the Dales Gorge Member of the Brockman Iron Formation and found N content and $\delta^{15}N$ value of 1.9 ppm and 11.5 ‰, respectively, within the range of the present data. In our sample set, N isotope values do not show any correlation with N content, C_{org}/N ratios (Fig. 7), or $\delta^{13}C_{org}$ values. The chemostratigraphic profile shows a generally inverse correlation between $\delta^{15}N$ and $\delta^{13}C_{carb}$ values (Fig. 4). However, a plot of $\delta^{15}N$ versus $\delta^{13}C_{carb}$ values does not clearly show any correlation between these two parameters (r^2 = 0.31; Fig. 7c), suggesting that they are only indirectly linked to each other.

5. Discussion

Before any discussion about paleoenvironmental implications of our results can take place, it is important to establish whether measured C and N contents and isotope compositions

404 preserved a primary signature, i.e., one generated in the water column, or one that has been
405 produced by later processes such as diagenesis or low-grade metamorphism.
406
407 *5.1. Evidence for primary C isotope composition of organic matter*
408
409 In sedimentary rocks, large variations in organic carbon content may reflect changes in (1)
410 primary productivity (i.e., production of microbial photoautotrophic biomass), (2) degree of
411 recycling of organic matter in the water column and in sediments during diagenesis, (3) extent of
412 thermal maturation of carbonaceous materials associated with sediment burial, and (4)
413 sedimentation rate resulting in organic matter dilution or concentration. These controls are further
414 explored below. Thermal maturation of organic molecules releases carbon (in the form of
415 hydrocarbons; e.g., CH_4), preferentially enriched in ^{12}C, and may lead to a significant decrease in
416 C_{org} content associated with an increase in $\delta^{13}C$ values of the residual organic matter (Hayes et al.,
417 1983). This isotope effect is small for metamorphic grades lower than the upper greenschist
418 facies (typically <2‰) and can thus be neglected in the present case since the Mount McRae
419 Shale and Brockman Iron Formation have experienced metamorphic temperatures <300°C
420 (Becker and Clayton, 1976; Smith et al., 1982; Kaufman et al., 1990, 2007). An important
421 observation for our samples is the relationship between C_{org} content and Fe/Ti molar ratios (Fig.
422 3a). Because Ti is immobile in any kind of aqueous fluid, the sedimentary flux of Ti mostly
423 reflects detrital contributions. If we assume a constant Fe/Ti molar ratio for the detrital source,
424 then an increase in Fe/Ti molar ratio in the sedimentary rocks will track an increase in the flux of
425 authigenic Fe (e.g., Dauphas et al., 2007a, 2007b). Accordingly, Fig. 3a shows that C_{org} content is
426 inversely proportional to the flux of authigenic Fe to the sediment. Previous studies of Archean

sedimentary rocks also identified an inverse relationship between C_{org} and Fe contents and proposed that it reflects the role of Fe-oxyhydroxides in mineralization of organic matter (e.g., Walker, 1984; Beukes et al., 1990; Kaufman et al., 1990; Bekker et al., 2010). In this scenario, ferric iron precipitate acts as an electron acceptor during early diagenesis for organic matter oxidation. This explanation is supported by the inverse correlation between C_{org} contents and Fe/Ti molar ratios (Fig. 3a), implying that C_{org} content was likely influenced to variable degree by organic-matter mineralization. An important question is whether this mineralization process imparted any modification to the C isotope composition of organic matter. If mineralization was associated with C isotope fractionation, then $\delta^{13}C$ values should show some correlation with C_{org} contents. This is not the case and in contrast to large variations in C_{org} content, $\delta^{13}C_{org}$ values of the Brockman Iron Formation show only moderate variability and can be regarded as constant at about -28.7 ± 0.8 ‰ (1σ). The possibility of a modern contamination — related to sampling or analytical procedures — with a source having a homogeneous $\delta^{13}C$ value seems unlikely, since C_{org} contents would be similar in all of the samples and would not show a stratigraphic trend (Fig. 4). The remarkable isotopic constancy for the whole range of lithologies suggests that modification of the $\delta^{13}C_{org}$ values was minor after sediment deposition. We therefore argue that the C isotope composition of organic matter measured in our study represents the primary organic carbon signature of the microorganisms thriving in the water column. The constancy of $\delta^{13}C_{org}$ values also indicates that C was assimilated from a homogeneous pool of dissolved inorganic carbon, with constant (or near constant) C isotope composition. The few samples of the Brockman Iron Formation significantly diverging from the mean $\delta^{13}C_{org}$ value may have organic matter generated via at least two different metabolic pathways imposing different carbon isotope fractionations. The chert sample (DGM307-6) has a particularly low C_{org} content and high $\delta^{13}C_{org}$ value of 0.05

wt% and -26.4 ‰, respectively, and could have been affected by intense loss of organic matter during diagenesis. Three samples in our study have $\delta^{13}C_{org}$ values significantly lower than the average $\delta^{13}C_{org}$ value of -28.7 ± 0.8 ‰ (samples DGM287, DGM288-1, and MR387). These lower $\delta^{13}C_{org}$ values are associated with high C_{org} contents (> 1wt%; see Table 2). On the stratigraphic profile (Fig. 4), they fit well with $\delta^{13}C_{org}$ values previously measured for the Mount McRae Shale, having even more negative values down-section (as low as -41.6 ‰; data from Kaufman et al., 2007 and Garvin et al., 2009). These negative $\delta^{13}C$ values have been related to the activity of methanotrophic organisms (Kaufman et al., 2007). Accordingly, our samples with markedly negative $\delta^{13}C_{org}$ values may also contain some organic matter derived from methanotrophic microbes.

5.2. Carbonate precipitation during diagenesis

Sedimentary carbonates record the isotopic composition of dissolved inorganic carbon (DIC) pool from which they precipitated with a positive offset of ~1 ‰ due to thermodynamic isotope equilibrium (e.g., Morse and Mackenzie, 1990; for siderite see Zhang et al., 2001, and references therein). Their $\delta^{13}C_{carb}$ and $\delta^{13}C_{org}$ values can be used to deduce the isotope fractionation associated with carbon assimilation ($\Delta^{13}C = \delta^{13}C_{carb} - \delta^{13}C_{org}$), which is a proxy for metabolic processes (e.g., Hayes et al., 1999; Bekker et al., 2001, 2008; Thomazo et al., 2009b; Bekker and Kaufman, 2007; Sansjofre et al., 2011).

In our samples of the Brockman Iron Formation, $\delta^{13}C_{org}$ values show little variation over the stratigraphic profile (Fig. 4). It implies that living organisms thrived in a homogeneous pool of dissolved inorganic carbon with a constant $\delta^{13}C$ value. In contrast, $\delta^{13}C_{carb}$ values show large

473 variability among the samples, implying that not all carbonates precipitated from the same pool
474 of dissolved inorganic carbon as that utilized by organic matter. A portion (if not all) of the
475 carbonates could have precipitated from either (1) a deep layer of the stratified water column
476 (Beukes et al., 1990), or (2) sediment porewaters during diagenesis (Walker, 1984). Petrographic
477 and geochemical data supports the second scenario. Petrographic observations show that many
478 carbonates in the Brockman Iron Formation cement matrix minerals, indicating that they formed
479 after sedimentary components were deposited. Another argument derives from the rough
480 correlation between C_{org} contents and $\delta^{13}C_{carb}$ values (Fig. 5). Low C_{org} content might reflect
481 mineralization of organic matter during sediment diagenesis (see discussion in section 5.1).
482 Correlation between C_{org} contents and $\delta^{13}C_{carb}$ values then may indicate that the more organic matter
483 was mineralized, the more negative $\delta^{13}C$ values were imprinted on carbonates. This can be
484 explained by a two-stage process: (1) organic matter degradation via ferric-oxyhydroxide
485 reduction, which increases ferrous iron and CO_2 content in solution as in the following reaction:

486 $$CH_2O + 8H^+ + 4Fe(OH)_3 \rightarrow 4Fe^{2+}_{aq} + CO_2 + 11H_2O \quad (1)$$

487 (2) precipitation of iron-rich carbonates from sediment pore-waters such as:

488 $$Fe^{2+}_{aq} + CO_2 + H_2O \rightarrow FeCO_3 + 2H^+ \quad (2)$$

489 Based on this model, we could expect a correlation between $\delta^{13}C_{carb}$ value and the amount or
490 proportion of siderite (or other Fe-carbonate) in our samples, as represented by the carbonate
491 fraction extracted at the temperature of ~130°C (Table 3). Such a correlation is not observed
492 possibly because many carbonates are not pure siderites but mixed Fe-Ca-Mg carbonates, which
493 may have formed during diagenesis or later by carbonate recrystallization during sediment burial.
494 In any case, it does not contradict the possibility of diagenetic carbonate formation during organic
495 matter degradation via ferric-oxyhydroxide reduction, but it suggests that diagenetic Fe-

carbonates are not exclusively siderites. A similar mechanism for carbonate precipitation was also inferred based on $\delta^{13}C$ data obtained for carbonates and organic matter from the Late Archean Transvaal Supergroup in South Africa (Fischer et al., 2009). It was also proposed based on coupling of Fe and C isotope values in the Late Archean carbonate-bearing iron formations (Heimann et al., 2010; Craddock and Dauphas, 2011), suggesting that this process could have been common during the Late Archean.

5.3. Preservation of N isotope signature in organic matter

Like for carbon, it is important to determine if N isotope composition reflects a signature of organisms living in the water column or was affected by late modifications related to post-depositional processes. This is crucial since late-stage hydrothermal processes have been invoked for iron formation in some localities within the Hamersley Province (Webb et al., 2003). Correlation between N and C_{org} contents suggests that N originated from organic matter (Fig. 6a). Since organic C is likely predominantly derived from primary producers, the same origin might equally apply to N. Samples from the Brockman Iron Formation have C_{org}/N molar ratios averaging 242 ± 200 (1σ), which is similar to the average C_{org}/N molar ratio of the previously measured Archean cherts from various localities including Western Australia, South Africa and Northern America (200.7 ± 137, 1σ, n=59; Beaumont and Robert, 1999; Ueno et al., 2004, Pinti et al., 2007, 2009). Similarly to carbon content, nitrogen content is negatively correlated with Fe/Ti molar ratio, suggesting that N was also removed from the sediment by organic matter mineralization (Fig. 3b; see discussion on organic carbon content in section 5.1). The lowest N

518 content corresponds to the chert sample DGM307-6 that contains ~1.3 ppm N, and is similar to
519 some other Archean chert samples in nitrogen content (Pinti et al., 2001, 2007, 2009).

520 Nitrogen content shows a broad positive correlation with K_2O content (Fig. 6b). This
521 suggests that part of the nitrogen released to sediment porewaters during organic matter
522 mineralization, was substituted in the form of NH_4^+ for K^+ in K-bearing minerals, because of their
523 similar charge and ionic radius (Honma and Itihara, 1981; Busigny et al., 2003a; Rouchon et al.,
524 2005). In other words, C and N were likely supplied from the same organic material but
525 diagenetic evolution induced a loss of N from organic matter with partial incorporation as NH_4^+
526 into K-minerals. Since N is preferentially released from organic matter during diagenesis and
527 metamorphism with respect to C, C/N ratio can be used as a proxy to evaluate the effect of these
528 processes on N content and its isotopic composition (Ader et al., 2006; Boudou et al., 2008).
529 Decrease in C/N ratio with increasing K_2O content confirms that part of the N released from
530 organic matter was fixed as NH_4^+ in K-silicates and was then protected from diagenesis and early
531 metamorphism (Fig. 6c). One banded iron formation sample (DGM364), plotting away from the
532 general K_2O-N trend, represents particularly high N content with respect to its K_2O and C_{org}
533 contents (83.9 ppm N, 0.12 wt% K_2O, and 0.59 wt% C_{org}; Fig. 6a and b). This sample shows the
534 highest Fe_{total} concentration, having 78.16 wt% Fe_2O_3. It might indicate that N was predominantly
535 bound with Fe oxides, as was earlier suggested by Pinti et al. (2007). Since N isotopes could be
536 fractionated during organic matter degradation, it is important to evaluate whether N isotope
537 signature of our samples records paleo-ecosystem and paleo-environmental (e.g., redox)
538 conditions. Organic matter degradation occurs (1) in the water column and in the sediment during
539 early diagenesis, and (2) during thermal maturation associated with burial diagenesis and
540 metamorphism. In oxic environments, early diagenesis may impart a shift in $\delta^{15}N_{org}$ values

541 towards more positive values with a magnitude reaching ~3 ‰ (e.g., Altabet and Francois, 1994;
542 Lehmann et al., 2002; Gaye et al., 2009; Möbius et al., 2010). In contrast, organic matter
543 degradation under anoxic and suboxic conditions either preserves original nitrogen isotope values
544 or slightly lowers $\delta^{15}N_{org}$ values with a shift smaller than 1 ‰ (e.g., Lehmann et al., 2002; Thunell
545 et al., 2004; Möbius et al., 2010). In the case of the Brockman Iron Formation, the deep waters of
546 the basin were clearly anoxic as indicated by (i) the particularly high Fe content in the sediments
547 requiring high dissolved Fe(II) concentrations, and (ii) REE patterns lacking a negative Ce
548 anomaly and with a pronounced positive Eu anomaly reflecting a source of reduced, high-
549 temperature fluids similar to modern, mid-ocean ridge hydrothermal systems (e.g., Klein and
550 Beukes, 1989; Alibert and McCulloch, 1993; Beukes and Gutzmer, 2008; Planavsky et al., 2010).
551 Accordingly, $\delta^{15}N$ values of our samples were probably not or only slightly modified during early
552 diagenesis in this anoxic depositional setting. Effect of thermal maturation associated with burial
553 diagenesis and metamorphism on N isotope composition can be tested using tracers such as N
554 concentration and C/N ratio. Studies on coal with variable maturity showed that as metamorphic
555 grade increases, organic N content decreases and C_{org}/N_{org} ratio increases, while $\delta^{15}N$ values remain
556 largely unaffected (Ader et al., 1998, 2006; Boudou et al., 2008). However, if N present in form
557 of NH_4^+ in silicate minerals is lost during metamorphism then the residual $\delta^{15}N$ values could be
558 increased by up to a few per mil (Bebout and Fogel, 1992; Mingram and Braüer, 2001; Bebout et
559 al., 1999; Busigny et al., 2003b; Jia, 2006). In our sample set, N contents and C/N ratios do not
560 show any significant correlation with $\delta^{15}N$ values (Fig. 7a and b), thus suggesting that $\delta^{15}N$ values
561 are not controlled by N loss during sediment burial and metamorphism. In support of this
562 statement, the stratigraphic trend of $\delta^{15}N$ values within the drill-core shows smooth alternating
563 rises and falls of $\delta^{15}N$ values suggesting either a secular or local control over N isotope variations

(Fig. 4) rather than that imposed by post-depositional modification. We conclude that the $\delta^{15}N$ and $\delta^{13}C_{org}$ values of our samples from the Brockman Iron Formation and Mount McRae Shale mostly reflect primary organic matter composition.

5.4. Implications for ancient N biogeochemical cycle

In this section, the elemental concentrations and isotopic variations of N-C_{org}-C_{carb}-Fe in the Mount McRae Shale and Brockman Iron Formation are integrated to explore several models of N biogeochemical cycle in the Late Archean ocean. For all herein discussed models, we assume the following lateral distribution of sedimentary facies from proximal to distal, deep-sea environments (cf., Beukes et al., 1990; Bekker et al., 2010): (1) organic matter-rich, sulfidic shales deposited under euxinic conditions, (2) iron-rich shales and carbonates, and (3) banded iron formations and chert in deeper settings (Fig. 8). Nutrients sustaining organic productivity were predominantly supplied from the continents or by coastal upwelling currents, resulting in higher organic productivity in proximal facies. Part of the Mount McRae Shale was deposited under euxinic conditions (Reinhard et al., 2009; Raiswell et al., 2011), where accumulation of free H_2S in the water column in excess of dissolved Fe^{2+} might have resulted from either riverine delivery of SO_4^{2-} produced by oxidative continental weathering or atmospheric supply of sulphate aerosols generated in the anoxic atmosphere by UV photolysis (Bekker et al., 2010), combined with bacterial SO_4^{2-} reduction associated with the remineralisation of organic matter. The Mount McRae Shale high organic productivity, reflected in its elevated C_{org} concentrations, is associated with markedly negative $\delta^{13}C_{org}$ values (Figure 4) suggesting high methanotrophic contributions to the organic matter (Kaufman et al., 2007). Methanotrophs have two specific requirements. First, a

587 flux of methane, likely derived from preferential organic matter mineralization by methanogens
588 under low oxygen conditions. For the Mount McRae Shale, the low Fe/Ti ratios (Figure 3)
589 indicate that ferric iron availability was limited, therefore favouring methanogenesis as the
590 dominant degradation pathway in the deeper part of the water column and in the sediment
591 porewaters. Second, methanotrophic organisms require oxidant availability so that methane is
592 oxidized via either anaerobic, with, for example, sulphate as an electron acceptor, or aerobic
593 oxidation (Hayes et al., 1983; Thomazo et al., 2009a). The upper part of the water column in the
594 Mount McRae Shale depositional environment therefore should have contained either dissolved
595 oxygen or another oxidant such as sulphate, nitrate, or Fe- and Mn-oxyhydroxides. In contrast to
596 the Mount McRae Shale, the biomass in the Brockman Iron Formation depositional setting was
597 probably dominated by photosynthetic organisms, either oxygenic or anoxygenic.
598 Chemoautotrophic organisms living in hydrothermal systems were also proposed as the main
599 source of organic matter for Archean cherts (Pinti and Hashizume, 2001; Pinti et al., 2001, 2009).
600 This source of organic carbon and nitrogen seems unlikely for our samples from the Brockman
601 Iron Formation both because of their geological setting (no evidence for active hydrothermal
602 systems at the depositional site of this unit) and their $\delta^{15}N$ and $\delta^{13}C$ values, which are not as
603 negative as those typical of chemoautotrophs (e.g., $\delta^{15}N$ values as low as -5 ‰ and $\delta^{13}C$ values
604 lower than -40 ‰). The $\delta^{13}C$ values of our samples (-28.7 ± 0.8 ‰; Fig. 4) are compatible with
605 primary producers living in the photic zone of the water column. The ferric iron flux to the
606 depositional site of the Brockman Iron Formation was obviously higher than that to the
607 depositional site of the Mount McRae Shale, as illustrated by their Fe/Ti ratios (Fig. 3). This
608 suggests that anaerobic respiration using iron oxyhydroxide reduction may have been the
609 dominant degradation pathway for organic matter, which is energetically more favourable than

methanogenesis. Iron oxyhydroxide reduction would have increased dissolved Fe(II) and DIC concentrations in porewaters, likely inducing Fe-rich carbonate precipitation with low $\delta^{13}C_{carb}$ values (see discussion in section 5.2). The chemostratigraphic profiles presented in Figure 4 show roughly inverse trends for $\delta^{15}N$ and $\delta^{13}C_{carb}$ values in the Brockman Iron Formation. Since $\delta^{13}C_{carb}$ values likely reflect a diagenetic origin of Fe-rich carbonates, $\delta^{15}N$ variations might be also interpreted as resulting from organic matter degradation. However, the discussion presented above in section 5.3 as well as a weak direct correlation between $\delta^{15}N$ and $\delta^{13}C_{carb}$ values (Fig. 7c) suggest that $\delta^{15}N$ values more likely represent the primary signature of organic matter in the water column, i.e. the N isotope composition of photosynthetic organisms. It seems likely therefore that N and C_{carb} isotope compositions were linked by indirect processes.

According to previous studies, two possible scenarios can be considered for the redox structure in the water column of the Late Archean oceans. In the first case, the water column is stratified with a thin oxygenated (oxic or disoxic) upper layer overlying an anoxic and ferruginous lower layer (e.g., Beukes and Gutzmer, 2008). This scenario is traditionally invoked to explain deposition of banded iron formations, where upwelling dissolved Fe(II) is oxidized with O_2 produced through photosynthetic activity of cyanobacteria (Cloud, 1973; Klein and Beukes, 1989). The second scenario infers a fully anoxic water column (e.g., Planavsky et al., 2010) with banded iron formation deposition controlled by one or several of the following processes: metabolic Fe(II) oxidation, UV photooxidation, or quantitative consumption of produced O_2 (e.g., Bekker et al., 2010). In both models for iron formation deposition, nitrogen from the atmosphere was initially introduced into the ocean by N_2-fixing organisms, such as cyanobacteria, under either aerobic or anaerobic conditions. Nitrogen assimilated by these organisms is not strongly fractionated in the modern ocean ($\delta^{15}N \approx 0$ ‰; e.g., Minagawa and

633 Wada, 1986), but can have negative values (as low as -3 ‰) when N_2-fixing organisms are grown
634 in Fe-enriched media (Zerkle et al., 2008). After death of N_2-fixing bacteria, they would sink
635 through the water column and would be incorporated into sediments resulting in $\delta^{15}N$ values of
636 sedimentary organic matter around 0 ‰. Nitrogen from their nucleic and amino acids can be
637 partially released as ammonium (NH_4^+) by mineralization in the water column or in sediments.
638 Further processing of NH_4^+ will depend on local redox conditions. The positive $\delta^{15}N$ values of the
639 Mount McRae Shale and Brockman Iron Formation indicate that N_2-fixing organisms were not
640 the only source of organic matter to the sediment. Positive $\delta^{15}N$ values of this magnitude in
641 Precambrian rocks can be caused by three different pathways: (1) partial assimilation of
642 ammonium (Papineau et al., 2009), (2) partial nitrification of ammonium, followed by complete
643 denitrification of the produced nitrite (Thomazo et al., 2011), and (3) quantitative oxidation of
644 ammonium to nitrate, followed by partial denitrification in the water column (Godfrey and
645 Falkowski, 2009; Garvin et al., 2009). The cases 1 and 2 require global anoxic conditions for
646 ammonium to be stable in the water column under open-marine conditions. In contrast, case 3
647 requires an oxic photic zone for nitrate stability, with limited denitrification under suboxic
648 conditions, similar to an oxygen minimum zone of the modern ocean. For all 3 cases, the rises
649 and falls of $\delta^{15}N$ values in the Mount McRae Shale and Brockman Iron Formation would be
650 produced by variations in the relative proportion of N_2-fixation and ^{15}N-enriched NO_3^- or NH_4^+
651 assimilation. The Mount McRae Shale has lower $\delta^{15}N$ values (the average is 3.8 ± 1.7 ‰, n = 82;
652 Garvin et al., 2009) than the Brockman Iron Formation (the average is 7.5 ± 2.7 ‰, n = 26; Fig.
653 4). The lower $\delta^{15}N$ values of the Mount McRae Shale might reflect a stronger contribution of N_2-
654 fixation with respect to NO_3^- or NH_4^+ assimilation, lowering $\delta^{15}N$ values towards 0 ‰ (Zerkle et al.,
655 2008), which is characteristic of marine areas with high organic productivity. In contrast, a lower

organic productivity at the depositional site of the Brockman Iron Formation would have left more dissolved NO_3^- or NH_4^+ available for assimilation, resulting in less intense N_2-fixation and higher $\delta^{15}N$ values of the biomass. In the following sections, the three cases will be further explored and their applicability to the Mount McRae Shale and Brockman Iron Formation will be evaluated.

5.4.1. Nitrogen cycle in fully anoxic and ferruginous ocean

Under fully anoxic conditions (Fig. 8), dissolved NH_4^+ would accumulate in the water column and would be readily assimilated by living organisms. Ammonium assimilation favours light N isotope, rendering the residual NH_4^+ enriched in ^{15}N (Papineau et al., 2009; Hadas et al., 2009). Assuming a maximum fractionation factor of 27 ‰ for NH_4^+ assimilation (Sigman et al., 2009) and an initial ammonium $\delta^{15}N$ value of 0 ‰, a Rayleigh distillation model requires that 70% of the initial ammonium has to be assimilated and transferred to the sediment before producing organic matter with $\delta^{15}N$ values of +5 ‰, similar to those found in the Mount McRae Shale and Brockman Iron Formation (Fig. 4). However, the cumulated fraction of organic matter with nitrogen assimilated via such a distillation process would have a mean $\delta^{15}N$ value around -20 ‰, which is not found in either the Mount McRae Shale or Brockman Iron Formation. Thus, partial assimilation of ammonium (case 1 hypothesis) is unlikely to explain the present results.

The second hypothesis is based on a partial oxidation of NH_4^+, followed by complete removal of the nitrite product (Thomazo et al., 2011). Partial oxidation of NH_4^+ leads to the production of isotopically light nitrite with a fractionation of 10 to 40 ‰ (Casciotti et al., 2003), while residual NH_4^+ becomes progressively enriched in heavy isotope. The light isotope is then

679 removed from the system by quantitative denitrification of nitrite to nitrogen gas (N_2). This
680 sequence of reactions occurs under anoxic conditions, but requires a flux of O_2 that is fully used
681 up. This is rarely observed in modern environments because of their highly oxygenated state.
682 However, a recent study of particulate organic matter in Lake Kinneret, Israel, found ^{15}N-
683 enrichment up to 15-30 ‰ due to partial nitrification of NH_4^+ (Hadas et al., 2009), demonstrating
684 the feasibility of this process. If the positive $\delta^{15}N$ values observed in the Mount McRae Shale and
685 Brockman Iron Formation are inherited from partial oxidation of NH_4^+, then this process also has
686 to explain the $\delta^{15}N$-$\delta^{13}C_{carb}$ co-variations observed along the chemostratigraphic profile (Fig. 4). One
687 possibility is that O_2 produced by oxygenic photosynthesis was utilized for both Fe oxidation and
688 partial NH_4^+ oxidation. If this is the case, the flux of Fe-oxyhydroxides, leading to organic matter
689 mineralization and Fe-carbonate precipitation, will roughly correspond with the degree of partial
690 NH_4^+ oxidation. Based on this scenario, an increase in $\delta^{15}N$ values would track an increase in the
691 O_2 production in the upper ocean. It is important to note that application of this model to the
692 open-marine depositional site of the Mount McRae Shale and Brockman Iron Formation requires
693 NH_4^+ stability in the water column and thus generally anoxic conditions, with some "oxygen
694 oases" generated by blooms of oxygenic photosynthesizers (Fig. 8a), inducing partial NH_4^+
695 oxidation.

696 If O_2 was entirely absent from this system, an alternative electron acceptor for NH_4^+
697 oxidation could have been ferric oxyhydroxides ($Fe(OH)_3$ in Fig. 8b) that were generated in
698 anoxic, ferruginous Archean oceans. Microbial oxidation of NH_4^+ with Fe(III) under anaerobic
699 conditions was recently demonstrated in wetland soils (Clément et al., 2005; Shrestha et al.,
700 2009), tropical upland soil slurries (Yang et al., 2012), and a sludge from a cattle waste treatment
701 plant (Sawayama, 2006), and was also shown to be thermodynamically feasible (Clément et al.,

2005). This reaction may have been important in the Archean biogeochemical N cycle and can be written as,

$$NH_4^+ + 6\ Fe(OH)_3 + 10\ H^+ \rightarrow NO_2^- + 6\ Fe^{2+} + 16\ H_2O \quad (3)$$

Following NH_4^+ oxidation, NO_2^- would be reduced to N_2 by denitrification or anammox processes, since it is unstable under anaerobic conditions. Direct NH_4^+ oxidation to N_2 is also energetically feasible, yielding up to 245 kJ/mol (Yang et al., 2012), through the following reaction:

$$NH_4^+ + 3\ Fe(OH)_3 + 5\ H^+ \rightarrow 0.5\ N_2 + 3\ Fe^{2+} + 9\ H_2O \quad (4)$$

Although the N isotope fractionation associated with NH_4^+ oxidation with Fe(III) is not known, it is reasonable to assume fractionations similar to those imposed by O_2-driven nitrification process (10 to 40 ‰; Casciotti et al., 2003), thus enriching the residual NH_4^+ in ^{15}N. This scenario could also provide an explanation for the roughly inverse trends of $\delta^{15}N$ and $\delta^{13}C_{carb}$ values (Fig. 4). The highest flux of Fe-oxyhydroxides would correspond to the highest rate of ammonium oxidation, resulting in both an increase in $\delta^{15}N$ values and early diagenetic organic matter mineralization with ferric iron. The latter process in turn would induce Fe-carbonate precipitation with negative $\delta^{13}C_{carb}$ values.

5.4.2. Nitrogen cycle in a redox-stratified ocean

In the oxic upper layer of a stratified water column (Fig. 8c), NH_4^+ would be quantitatively oxidized to NO_3^- by nitrification, thus preventing any nitrogen isotope fractionation. In oxygen-minimum zones, or at redox boundaries, partial denitrification would increase the $\delta^{15}N$ value of residual NO_3^- (see review in Sigman et al., 2009). Assimilation of this residual NO_3^- by living organisms would transfer positive N isotope signature to the sedimentary deposit. Such a scenario

of a redox-stratified ocean has been proposed in previous studies to explain positive $\delta^{15}N$ values in Archean sedimentary rocks (Garvin et al., 2009; Godfrey and Falkowski, 2009). This scenario can be extended to the sedimentary sequence of the Brockman Iron Formation if it can explain the coupling between N and Fe biogeochemical cycles in the water column, which is required to establish the $\delta^{15}N$-$\delta^{13}C_{carb}$ co-variation (Fig. 4). One possibility is that partial denitrification of NO_3^- was mediated by anaerobic microbial oxidation of Fe(II) to Fe(III) (Shen et al., 2006). The corresponding reaction can be written as,

$$2NO_3^- + 10\ Fe^{2+} + 24\ H_2O \rightarrow\ N_2 + 10\ Fe(OH)_3 + 18\ H^+ \qquad (5)$$

The existence of anaerobic nitrate-dependant microbial Fe(II)-oxidation has been demonstrated by laboratory experiments (Straub et al., 1996), but data on N isotope fractionations associated with this process are still lacking. If partial denitrification via this process increases $\delta^{15}N$ values of residual NO_3^-, as it does in modern marine oxygen-minimum zones (Sigman et al., 2009), then assimilation of the ^{15}N-enriched residual NO_3^- would generate a pool of organic matter with positive $\delta^{15}N$ values. According to this reaction, the higher fluxes of $Fe(OH)_3$ to the sediment, possibly inducing diagenetic Fe-carbonate precipitation, would be associated with more positive $\delta^{15}N$ values in the sedimentary organic matter. Dissolved NO_3^- would be in contact with Fe^{2+} only at the redox boundary between upper oxygenated and lower anoxic layers in a stratified water column (Fig. 8c). Away from the redox boundary, Fe^{2+} would be immediately oxidized to Fe^{3+} under fully oxic conditions, and NO_3^- would be quantitatively denitrified under anoxic conditions. Although redox-stratified water column allows for an inverse relationship between $\delta^{15}N$ and $\delta^{13}C_{carb}$ values, as in the Brockman Iron Formation (Fig. 4), the feasibility of this model can be questioned. Based on this scenario, the flux of Fe oxyhydroxides to the sediments has to be balanced by NO_3^- denitrification. The reaction (5) presented above indicates that 1 mole of NO_3^- is

748 required for the oxidation of 5 moles of Fe^{2+}. However, considering the large flux of Fe associated
749 with deposition of banded iron formation, NO_3^- denitrification would have led to extensive,
750 probably quantitative, loss of dissolved NO_3^- to gaseous N_2. As a result of its low concentration,
751 the residual pool of partially denitrified NO_3^- at the redox boundary would have a negligible
752 impact on the NO_3^- inventory of the upper oxygenated ocean and, more specifically, on the N
753 isotope composition of the NO_3^--assimilating organisms. The feasibility of this redox-stratified
754 model should be further tested with a detailed dispersion-reaction model coupling N-C-Fe
755 biogeochemical cycles in the water column.
756
757 **6. Conclusion**
758
759 We propose herein that N and Fe biogeochemical cycles in the Late Archean open-marine
760 basin of the Hamersley Province were linked via redox reactions in the water column, and are
761 recorded by inverse co-variations between $\delta^{15}N$ and $\delta^{13}C_{carb}$ values in the Brockman Iron Formation.
762 Like in the Phanerozoic, N was probably introduced to the ocean mainly via N_2-fixation leading
763 to $\delta^{15}N$ values close to 0 ‰ in organic matter and NH_4^+ released during mineralization of organic
764 matter. Several scenarios based on different redox structures of the water column can satisfy the
765 literature and our own N isotope data. If the water column was anoxic, NH_4^+ would have been the
766 dominant species of dissolved nitrogen available for assimilation in the photic zone. Positive $\delta^{15}N$
767 values in this case would represent partial oxidation of NH_4^+, by either (1) O_2-controlled
768 nitrification, or (2) microbial oxidation with ferric oxyhydroxides, and subsequent quantitative
769 denitrification of NO_2^- and NO_3^- products. If the water column was redox-stratified, with an oxic
770 layer covering anoxic deep waters, N assimilated by primary producers would have been mostly

771 in the form of NO_3^- like in the Phanerozoic oceans. In this case, the positive $\delta^{15}N$ values would
772 have been produced by partial denitrification of NO_3^- coupled to anaerobic microbial oxidation of
773 ferrous to ferric iron. Accordingly, similar positive $\delta^{15}N$ values may record very different N
774 biogeochemical cycles under anoxic, redox-stratified, or fully oxic conditions in the oceans. We
775 emphasize therefore that N isotopes alone cannot be used to constrain the redox structure of the
776 ancient oceans, but can still be useful to address this question if utilized in combination with
777 other elemental and isotopic tracers.

778 As a perspective, we also point out the need to determine experimentally N isotope
779 fractionations associated with microbial redox reactions involving N and Fe cycles, such as NH_4^+
780 oxidation by ferric oxyhydroxides and/or denitrification of NO_3^- mediated by anaerobic oxidation
781 of Fe(II) to Fe(III). This may help future studies for seeking ancient traces of life in the Archean
782 geological record.

783

784 **Acknowledgements**

785 This work was partly funded by the INSU-PNP program of the CNRS and by the BQR grants of
786 IPGP. Colleagues from the Isotope Geochemistry Laboratories in IPGP are thanked for fruitful
787 discussions, particularly Pierre Cartigny, Magali Bonifacie, Pierre Sans-Jofre and Jabrane Labidi.
788 Michel Girard, Jean-Jacques Bourrand, Carine Chaduteau and Guillaume Landais are
789 acknowledged for their technical assistance. Marc Quintin is thanked for making thin sections of
790 all samples. AB contribution was supported by NSF and NSERC Discovery grants. Greame
791 Broadbent from Rio Tinto Exploration is thanked for access to drill cores and geological
792 information. Jim Kasting is thanked for handling the manuscript and three anonymous reviewers

793 are greatly acknowledged for their detailed comments. Contribution IPGP No. XXX and CNRS
794 No. XXX.

795

796 **References**

797

798 Ader, M., Boudou, J.P., Javoy, M., Goffe, B. and Daniels, E., 1998. Isotope study on organic
799 nitrogen of Westphalian anthracites from the western middle field of Pennsylvania (USA)
800 and from the Bramsche massif (Germany). Organic Geochemistry 29, 315-323.
801 Ader, M., Cartigny, P., Boudou, J.P., Oh, J.H., Petit, E. and Javoy, M., 2006. Nitrogen isotopic
802 evolution of carbonaceous matter during metamorphism: Methodology and preliminary
803 results. Chemical Geology 232, 152-169.
804 Ader, M., Macouin, M., Trindade, R.I.F., Hadrien, M.H., Yang, Z., Sun, Z. and Besse, J., 2009. A
805 multilayered water column in the Ediacaran Yangtze platform? Insights from carbonate
806 and organic matter paired $\delta^{13}C$. Earth and Planetary Science Letters 288, 213-227.
807 Alibert, C., and McCulloch, M. T., 1993. Rare element and neodymium isotopic compositions of
808 the banded iron-formations and associated shales from Hamersley, western Australia.
809 Geochimica Cosmochimica Acta 57, 187-204.
810 Altabet, M.A. and Francois, R., 1994. Sedimentary nitrogen isotopic ratio as a recorder for
811 surface ocean nitrate utilization. Global Biogeochemical Cycles 8, 103-116.
812 Anbar, A.D., Duan, Y., Lyons, T.W., Arnold, G.L., Kendall, B., Creaser, R.A., Kaufman, A.J.,
813 Gordon, G.W., Scott, C., Garvin, J. and Buick, R., 2007. A whiff of oxygen before the
814 Great Oxidation Event? Science 317, 1903-1906.
815 Anbar, A.D. and Knoll, A.H., 2002. Proterozoic ocean chemistry and evolution: A bioinorganic
816 bridge? Science 297, 1137-1142.
817 Beaumont, V. and Robert, F., 1999. Nitrogen isotope ratios of kerogens in Precambrian cherts: a
818 record of the evolution of atmosphere chemistry? Precambrian Research 96, 63-82.
819 Bebout, G.E., Cooper, D.C., Bradley, A.D. and Sadofsky, S.J., 1999. Nitrogen-isotope record of
820 fluid-rock interactions in the Skiddaw Aureole and granite, English Lake District.
821 American Mineralogist 84, 1495-1505.
822 Bebout, G.E. and Fogel, M.L., 1992. Nitrogen-isotope compositions of metasedimentary rocks in
823 the Catalina Schist, California - Implications for metamorphic devolatilization history.
824 Geochimica Et Cosmochimica Acta 56, 2839-2849.
825 Becker, R.H. and Clayton, R.N., 1976. Oxygen isotope study of a Precambrian Banded Iron-
826 Formation, Hamersley Range, Western-Australia. Geochimica et Cosmochimica Acta 40,
827 1153-1165.
828 Bekker, A., Kaufman, A.J., Karhu, J.A., Beukes, N.J., Swart, Q.D., Coetzee, L.L. and Eriksson,
829 K.A., 2001. Chemostratigraphy of the paleoproterozoic Duitschland Formation, South
830 Africa: Implications for coupled climate change and carbon cycling. American Journal of
831 Science 301, 261-285.
832 Bekker, A., Holland, H.D., Wang, P.L., Rumble, D., Stein, H.J., Hannah, J.L., Coetzee, L.L. and
833 Beukes, N.J., 2004. Dating the rise of atmospheric oxygen. Nature 427, 117-120.

834 Bekker, A. and Kaufman, A.J., 2007. Oxidative forcing of global climate change: A
835 biogeochemical record across the oldest Paleoproterozoic ice age in North America. Earth
836 and Planetary Science Letters 258, 486-499.
837 Bekker, A., Slack, J.F., Planavsky, N., Krapez, B., Hofmann, A., Konhauser, K.O. and Rouxel,
838 O.J., 2010. Iron Formation: The sedimentary product of a complex interplay among
839 mantle, tectonic, oceanic, and biospheric processes. Economic Geology 105, 467-508.
840 Beukes, N.J. and Gutzmer, J., 2008. Origin and paleoenvironmental significance of major Iron
841 Formations at the Archean-Paleoproterozoic boundary, Banded Iron Formation-Related
842 High-Grade Iron Ore. Reviews in Economic Geology, pp. 5-47.
843 Beukes, N.J., Klein, C., Kaufman, A.J. and Hayes, J.M., 1990. Carbonate petrography, kerogen
844 distribution, and carbon and oxygen isotope variations in an Early Proterozoic transition
845 from limestone to iron-formation deposition, Transvaal Supergroup, South-Africa.
846 Economic Geology 85, 663-690.
847 Blake, T. S. and Barley, M. E., 1992. Tectonic evolution of the Late Archaean to Early Proterozoic
848 Mount Bruce Megasequence Set, Western Australia. Tectonics 11, 1415-1425.
849 Boudou, J.P., Schimmelmann, A., Ader, M., Mastalerz, M., Sebilo, M. and Gengembre, L., 2008.
850 Organic nitrogen chemistry during low-grade metamorphism. Geochimica et
851 Cosmochimica Acta 72, 1199-1221.
852 Boyd, S.R., 2001. Ammonium as a biomarker in Precambrian metasediments. Precambrian
853 Research 108, 159-173.
854 Brandes, J.A., Devol, A.H. and Deutsch, C., 2007. New developments in the marine nitrogen
855 cycle. Chemical Reviews 107, 577-589.
856 Busigny, V., Ader, M. and Cartigny, P., 2005. Quantification and isotopic analysis of nitrogen in
857 rocks at the ppm level using sealed tube combustion technique: A prelude to the study of
858 altered oceanic crust. Chemical Geology 223, 249-258.
859 Busigny, V., Cartigny, P., Philippot, P. and Javoy, M., 2003a. Ammonium quantification in
860 muscovite by infrared spectroscopy. Chemical Geology 198, 21-31.
861 Busigny, V., Cartigny, P., Philippot, P., Ader, M. and Javoy, M., 2003b. Massive recycling of
862 nitrogen and other fluid-mobile elements (K, Rb, Cs, H) in a cold slab environment:
863 evidence from HP to UHP oceanic metasediments of the Schistes Lustres nappe (western
864 Alps, Europe). Earth and Planetary Science Letters 215, 27-42.
865 Canfield, D.E., Glazer, A.N. and Falkowski, P.G., 2010. The evolution and future of Earth's
866 nitrogen cycle. Science 330, 192-196.
867 Casciotti, K.L., Sigman, D.M. and Ward, B.B., 2003. Linking diversity and stable isotope
868 fractionation in ammonia-oxidizing bacteria. Geomicrobiology Journal 20, 335-353.
869 Clement, J.C., Shrestha, J., Ehrenfeld, J.G. and Jaffe, P.R., 2005. Ammonium oxidation coupled
870 to dissimilatory reduction of iron under anaerobic conditions in wetland soils. Soil
871 Biology & Biochemistry 37, 2323-2328.
872 Cloud, P., 1973. Paleoecological Significance of Banded Iron-Formation. Economic Geology 68,
873 1135-1143.
874 Craddock, P.R. and Dauphas, N., 2011. Iron and carbon isotope evidence for microbial iron
875 respiration throughout the Archean. Earth and Planetary Science Letters 303, 121-132.
876 Dauphas, N., Cates, N.L., Mojzsis, S.J. and Busigny, V., 2007a. Identification of chemical
877 sedimentary protoliths using iron isotopes in the > 3750 Ma Nuvvuagittuq supracrustal
878 belt, Canada. Earth and Planetary Science Letters 254, 358-376.

879 Dauphas, N., van Zuilen, M., Busigny, V., Lepland, A., Wadhwa, M. and Janney, P.E., 2007b.
880 Iron isotope, major and trace element characterization of early Archean supracrustal rocks
881 from SW Greenland: Protolith identification and metamorphic overprint. Geochimica et
882 Cosmochimica Acta 71, 4745-4770.
883 Fischer, W.W., Schroeder, S., Lacassie, J.P., Beukes, N.J., Goldberg, T., Strauss, H., Horstmann,
884 U.E., Schrag, D.P. and Knoll, A.H., 2009. Isotopic constraints on the Late Archean
885 carbon cycle from the Transvaal Supergroup along the western margin of the Kaapvaal
886 Craton, South Africa. Precambrian Research 169, 15-27.
887 Garvin, J., Buick, R., Anbar, A.D., Arnold, G.L. and Kaufman, A.J., 2009. Isotopic evidence for
888 an aerobic nitrogen cycle in the latest Archean. Science 323, 1045-1048.
889 Gaye, B., Wiesner, M.G. and Lahajnar, N., 2009. Nitrogen sources in the South China Sea, as
890 discerned from stable nitrogen isotopic ratios in rivers, sinking particles, and sediments.
891 Marine Chemistry 114, 72-85.
892 Godfrey, L.V. and Falkowski, P.G., 2009. The cycling and redox state of nitrogen in the
893 Archaean ocean. Nature Geoscience 2, 725-729.
894 Guo, Q.J., Strauss, H., Kaufman, A.J., Schroder, S., Gutzmer, J., Wing, B., Baker, M.A., Bekker,
895 A., Jin, Q.S., Kim, S.T. and Farquhar, J., 2009. Reconstructing Earth's surface oxidation
896 across the Archean-Proterozoic transition. Geology 37, 399-402.
897 Hadas, O., Altabet, M.A. and Agnihotri, R., 2009. Seasonally varying nitrogen isotope
898 biogeochemistry of particulate organic matter in Lake Kinneret, Israel. Limnology and
899 Oceanography 54, 75-85.
900 Hayes, J.M., Kaplan, I.R. and Wedeking, W., 1983. Geochemical evidence bearing on the origin
901 of aerobiosis, a speculative hypothesis. In: S.J. W. (Editor), Earth's earliest biosphere, its
902 origin and evolution. Princeton University Press, Princeton.
903 Hayes, J. M., Strauss, H., and Kaufman, A. J., 1999. The abundance of ^{13}C in marine organic
904 matter and isotopic fractionation in the global biogeochemical cycle of carbon during the
905 past 800 Ma. Chemical Geology 161, 103-125.
906 Heimann, A., Johnson, C.M., Beard, B.L., Valley, J.W., Roden, E.E., Spicuzza, M.J. and Beukes,
907 N.J., 2010. Fe, C, and O isotope compositions of banded iron formation carbonates
908 demonstrate a major role for dissimilatory iron reduction in similar to 2.5 Ga marine
909 environments. Earth and Planetary Science Letters 294, 8-18.
910 Holland, H.D., 1984. The chemical evolution of the atmosphere and oceans. Princeton University
911 Press, Princeton, 582 pp.
912 Holland, H.D., 2002. Volcanic gases, black smokers, and the Great Oxidation Event. Geochimica
913 Et Cosmochimica Acta 66, 3811-3826.
914 Holland, H.D., 2006. The oxygenation of the atmosphere and oceans. Philosophical Transactions
915 of the Royal Society B 361, 903–915.
916 Holland, H.D., 2009. Why the atmosphere became oxygenated: A proposal. Geochimica Et
917 Cosmochimica Acta 73, 5241-5255.
918 Honma, H. and Itihara, Y., 1981. Distribution of ammonium in minerals of metamorphic and
919 granitic-rocks. Geochimica Et Cosmochimica Acta 45, 983-988.
920 Jia, Y.F., 2006. Nitrogen isotope fractionations during progressive metamorphism: A case study
921 from the Paleozoic Cooma metasedimentary complex, southeastern Australia.
922 Geochimica Et Cosmochimica Acta 70, 5201-5214.
923 Jia, Y.F. and Kerrich, R., 2004a. A reinterpretation of the crustal N-isotope record: evidence for a
924 N-15-enriched Archean atmosphere? Terra Nova 16, 102-108.

925 Jia, Y.F. and Kerrich, R., 2004b. Nitrogen 15-enriched Precambrian kerogen and hydrothermal
926 systems. Geochemistry Geophysics Geosystems 5, Q07005, doi:10.1029/2004GC000716.
927 Junuium, C.K., and Arthur, M.A., 2007. Nitrogen cycling during the Cretaceous, Cenomanian-
928 Turonian Oceanic Anoxic Event II. Geochemistry Geophysics Geosystems 8, Q03002,
929 doi:10.1029/2006GC001328
930 Kappler, A., Pasquero, C., Konhauser, K.O. and Newman, D.K., 2005. Deposition of banded iron
931 formations by anoxygenic phototrophic Fe(II)-oxidizing bacteria. Geology 33, 865-868.
932 Kaufman, A.J., Hayes, J.M. and Klein, C., 1990. Primary and diagenetic controls of isotopic
933 compositions of iron-formation carbonates. Geochimica et Cosmochimica Acta 54, 3461-
934 3473.
935 Kaufman, A.J., Johnston, D.T., Farquhar, J., Masterson, A.L., Lyons, T.W., Bates, S., Anbar,
936 A.D., Arnold, G.L., Garvin, J. and Buick, R., 2007. Late Archean biospheric oxygenation
937 and atmospheric evolution. Science 317, 1900-1903.
938 Kendall, C. and Grim, E., 1990. Combustion tube method for measurement of nitrogen isotope
939 ratios using calcium-oxide for total removal of carbon-dioxide and water. Analytical
940 Chemistry 62, 526-529.
941 Konhauser, K.O., Hamade, T., Raiswell, R., Morris, R.C., Ferris, F.G., Southam, G. and
942 Canfield, D.E., 2002. Could bacteria have formed the Precambrian banded iron
943 formations? Geology 30, 1079-1082.
944 Krapež, B., Barley, M.E. and Pickard, A.L., 2003. Hydrothermal and resedimented origins of the
945 precursor sediments to banded iron formation: sedimentological evidence from the Early
946 Palaeoproterozoic Brockman Supersequence of Western Australia. Sedimentology 50,
947 979-1011.
948 Lehmann, M.F., Bernasconi, S.M., Barbieri, A. and McKenzie, J.A., 2002. Preservation of
949 organic matter and alteration of its carbon and nitrogen isotope composition during
950 simulated and in situ early sedimentary diagenesis. Geochimica et Cosmochimica Acta
951 66, 3573-3584.
952 Marty, B., Zimmermann, L., Pujol, M., Burgess, R. and Philippot, P., 2012. Nitrogen
953 composition of the ancient atmosphere from fluid inclusion analysis of Archean quartz.
954 Mineralogical Magazine, Goldschmidt Conference Abstracts, p. 65.
955 McCrea, J.M., 1950. On the isotopic chemistry of carbonates and a paleotemperature scale.
956 Journal of Chemical Physics 18, 849-857.
957 Minagawa, M. and Wada, E., 1986. Nitrogen isotope ratios of red tide organisms in the East-
958 China sea - a characterization of biological nitrogen-fixation. Marine Chemistry 19, 245-
959 259.
960 Mingram, B. and Brauer, K., 2001. Ammonium concentration and nitrogen isotope composition
961 in metasedimentary rocks from different tectonometamorphic units of the European
962 Variscan Belt. Geochimica et Cosmochimica Acta 65, 273-287.
963 Miyano, T. and Klein, C., 1989. Phase-equilibria in the system K2O-FeO-Mgo-Al2O3-SiO2-
964 H2O-CO2 and the stability limit of stilpnomelane in metamorphosed precambrian iron-
965 formations. Contributions to Mineralogy and Petrology 102, 478-491.
966 Möbius, J., Lahajnar, N. and Emeis, K.C., 2010. Diagenetic control of nitrogen isotope ratios in
967 Holocene sapropels and recent sediments from the Eastern Mediterranean Sea.
968 Biogeosciences 7, 3901-3914.

969 Möbius, J., 2013. Isotope fractionation during nitrogen remineralization (ammonification):
970 Implications for nitrogen isotope biogeochemistry. Geochimica et Cosmochimica Acta
971 105, 422-432.
972 Morse, J.W. and Mackenzie, F.T., 1990. Geochemistry of sedimentary carbonates. Developents
973 in sedimentology 48. Elsevier, 681 pp.
974 Murakami, T., Sreenivas, B., Das Sharma, S. and Sugimori, H., 2011. Quantification of
975 atmospheric oxygen levels during the Paleoproterozoic using paleosol compositions and
976 iron oxidation kinetics. Geochimica Et Cosmochimica Acta 75, 3982-4004.
977 Papineau, D., Mojzsis, S.J., Karhu, J.A. and Marty, B., 2005. Nitrogen isotopic composition of
978 ammoniated phyllosilicates: case studies from Precambrian metamorphosed sedimentary
979 rocks. Chemical Geology 216, 37-58.
980 Papineau, D., Purohit, R., Goldberg, T., Pi, D.H., Shields, G.A., Bhu, H., Steele, A. and Fogel,
981 M.L., 2009. High primary productivity and nitrogen cycling after the Paleoproterozoic
982 phosphogenic event in the Aravalli Supergroup, India. Precambrian Research 171, 37-56.
983 Pecoits, E., Gingras, M.K., Barley, M.E., Kappler, A., Posth, N.R. and Konhauser, K.O., 2009.
984 Petrography and geochemistry of the Dales Gorge banded iron formation: Paragenetic
985 sequence, source and implications for palaeo-ocean chemistry. Precambrian Research
986 172, 163-187.
987 Pickard, A.L., Barley, M.E. and Krapez, B., 2004. Deep-marine depositional setting of banded
988 iron formation: sedimentological evidence from interbedded clastic sedimentary rocks in
989 the early Palaeoproterozoic Dales Gorge Member of Western Australia. Sedimentary
990 Geology 170, 37-62.
991 Pinti, D.L. and Hashizume, K., 2001. 15N-depleted nitrogen in Early Archean kerogens: clues on
992 ancient marine chemosynthetic-based ecosystems? A comment to Beaumont,V.,
993 Robert,F., 1999. Precambrian Res. 96, 62-82. Precambrian Research 105, 85-88.
994 Pinti, D.L., Hashizume, K. and Matsuda, J., 2001. Nitrogen and argon signatures in 3.8 to 2.8 Ga
995 metasediments: Clues on the chemical state of the Archean ocean and the deep biosphere.
996 Geochimica Et Cosmochimica Acta 65, 2301-2315.
997 Pinti, D.L., Hashizume, K., Orberger, B., Gallien, J.P., Cloquet, C. and Massault, M., 2007.
998 Biogenic nitrogen and carbon in Fe-Mn-oxyhydroxides from an Archean chert, Marble
999 Bar, Western Australia. Geochemistry Geophysics Geosystems 8.
1000 Pinti, D.L., Hashizume, K., Sugihara, A., Massault, M. and Philippot, P., 2009. Isotopic
1001 fractionation of nitrogen and carbon in Paleoarchean cherts from Pilbara craton, Western
1002 Australia: Origin of N-15-depleted nitrogen. Geochimica et Cosmochimica Acta 73,
1003 3819-3848.
1004 Planavsky, N., Bekker, A., Rouxel, O.J., Kamber, B., Hofmann, A., Knudsen, A. and Lyons,
1005 T.W., 2010. Rare Earth Element and yttrium compositions of Archean and
1006 Paleoproterozoic Fe formations revisited: New perspectives on the significance and
1007 mechanisms of deposition. Geochimica et Cosmochimica Acta 74, 6387-6405.
1008 Prokopenko, M.G., Hammond, D.E., Berelson, W.M., Bernhard, J.M., Stott, L. and Douglas, R.,
1009 2006. Nitrogen cycling in the sediments of Santa Barbara basin and Eastern Subtropical
1010 North Pacific: Nitrogen isotopes, diagenesis and possible chemosymbiosis between two
1011 lithotrophs (Thioploca and Anammox) - "riding on a glider". Earth and Planetary Science
1012 Letters 242, 186-204.
1013 Raiswell, R., Reinhard, C.T., Derkowski, A., Owens, J., Bottrell, S.H., Anbar, A.D. and Lyons,
1014 T.W., 2011. Formation of syngenetic and early diagenetic iron minerals in the late

Archean Mt. McRae Shale, Hamersley Basin, Australia: New insights on the patterns, controls and paleoenvironmental implications of authigenic mineral formation. Geochimica et Cosmochimica Acta 75, 1072-1087.

Rasmussen, B., Meier, D.B., and Krapež, B., 2013. Iron silicate microgranules as precursor sediments to 2.5-billion-year-old banded iron formations. Geology 41, 435-438.

Rasmussen, B., Blake, T.S. and Fletcher, I.R., 2005. U-Pb zircon age constraints on the Hamersley spherule beds: Evidence for a single 2.63 Ga Jeerinah-Carawine impact ejecta layer. Geology 33, 725-728.

Rau, G.H., Arthur, M.A., and Dean, W.E., 1987. $^{15}N/^{14}N$ variations in Cretaceous Atlantic sedimentary sequences: implication for past changes in marine nitrogen biogeochemistry. Earth and Planetary Science Letters 82, 269-279.

Reinhard, C.T., Raiswell, R., Scott, C., Anbar, A.D. and Lyons, T.W., 2009. A late Archean sulfidic sea stimulated by early oxidative weathering of the continents. Science 326, 713-716.

Rosenbaum, J. and Sheppard, S.M.F., 1986. An isotopic study of siderites, dolomites and ankerites at high-temperatures. Geochimica et Cosmochimica Acta 50, 1147-1150.

Rouchon, V., Pinti, D.L., Gallien, J.P., Orberger, B., Daudin, L., and Westall, F. (2005) NRA analyses of N and C in hydromuscovite aggregates from a 3.5 Ga chert from Kittys Gap, Pilbara, Australia. Nuclear Instruments and Methods in Physics Research B 231, 536–540.

Sansjofre, P., Ader, M., Trindade, R.I.F., Elie, M., Lyons, J., Cartigny, P. and Nogueira, A.C.R., 2011. A carbon isotope challenge to the Snowball Earth. Nature 478, 93-97.

Sawayama, S., 2006. Possibility of anoxic ferric ammonium oxidation. Journal of Bioscience and Bioengineering 101, 70-72.

Scott, C.T., Bekker, A., Reinhard, C.T., Schnetger, B., Krapez, B., Rumble, D. and Lyons, T.W., 2011. Late Archean euxinic conditions before the rise of atmospheric oxygen. Geology 39, 119-122.

Shen, Y., Pinti, D.L., and Hashizume, K., 2006. Biogeocgemical cycles of sulfur and nitrogen in the Archean ocean and atmosphere. In: K. Benn, J.C. Mareschal and K.C. Condie (Editors), Archean Geodynamics and Environments. American Geophysical Union, Washington D.D. Geophysical Monograph 164, 305–320.

Shrestha, J., Rich, J.J., Ehrenfeld, J.G. and Jaffe, P.R., 2009. Oxidation of ammonium to nitrite under iron-reducing conditions in wetland soils laboratory, field demonstrations, and push-pull rate determination. Soil Science 174, 156-164.

Sigman, D.M., Karsh, K.L. and Casciotti, K.L., 2009. Nitrogen isotopes is the ocean. In: J.H. Steele, T. S.A. and K.K. Turekian (Editors), Encyclopedia of Ocean Sciences. Academic Press, Oxford, pp. 40-54.

Smith, R. E., Perdrix, J. L., and Parks, T. C., 1982. Burial metamorphism in the Hamersley Basin, Western Australia. Journal of Petrology 23, 75-102.

Straub, K.L., Benz, M., Schink, B., and Widdel, F., 1996. Anaerobic, nitrate dependent microbial oxidation of ferrous iron. Applied and Environmental Microbiology 62, 1458-1460.

Thomazo, C., Ader, M., Farquhar, J. and Philippot, P., 2009a. Methanotrophs regulated atmospheric sulfur isotope anomalies during the Mesoarchean (Tumbiana Formation, Western Australia). Earth and Planetary Science Letters 279, 65-75.

Thomazo, C., Pinti, D.L., Busigny, V., Ader, M., Hashizume, K. and Philippot, P., 2009b. Biological activity and the Earth's surface evolution: Insights from carbon, sulfur,

nitrogen and iron stable isotopes in the rock record. Comptes Rendus Palevol 8, 665-678.
Thomazo, C., Ader, M. and Philippot, P., 2011. Extreme ^{15}N-enrichments in 2.72-Gyr-old sediments: evidence for a turning point in the nitrogen cycle. Geobiology 9, 107-120.
Thunell, R.C., Sigman, D.M., Muller-Karger, F., Astor, Y. and Varela, R., 2004. Nitrogen isotope dynamics of the Cariaco Basin, Venezuela. Global Biogeochemical Cycles 18.
Tolstikhin, I.N. and Marty, B., 1998. The evolution of terrestrial volatiles: a view from helium, neon, argon and nitrogen isotope modelling. Chemical Geology 147, 27-52.
Trendall, A.F. and Blockley, J.G., 1970. The iron formations of the Precambrian Hamersley Group of Western Australia, with special reference to crocidolite. Bull. Geol. Surv. West. Aust. 119, 366 pp.
Trendall, A.F., Compston, W., Nelson, D.R., De Laeter, J.R. and Bennett, V.C., 2004. SHRIMP zircon ages constraining the depositional chronology of the Hamersley Group, Western Australia. Australian Journal of Earth Sciences 51, 621-644.
Ueno, Y., Yoshioka, H., Maruyama, S. and Isosaki, Y., 2004. Carbon isotopes and Petrography of kerogens in ~3.5-Ga hydrothermal silica dikes in the North Pole area, Western Australia. Geochimica et Cosmochimica Acta 68, 573-589.
Wada, E., Kadonaga, T. and Matsuo, S., 1975. 15N abundance in nitrogen of naturally occuring substances and global assessment of denitrification from isotopic vewpoint. Geochemical Journal 9, 139-148.
Walker, J.C.G., 1984. Suboxic Diagenesis in Banded Iron Formations. Nature 309, 340-342.
Webb, A.D., Dickens, G.R. and Oliver, N.H.S., 2003. From banded iron-formation to iron ore: geochemical and mineralogical constraints from across the Hamersley Province, Western Australia. Chemical Geology 197, 215-251.
Yang, W.H., Weber, K.A. and Silver, W.L., 2012. Nitrogen loss from soil through anaerobic ammonium oxidation coupled to iron reduction. Nature Geoscience 5, 538-541.
Zerkle, A.L., Junium, C.K., Canfield, D.E. and House, C.H., 2008. Production of 15N-depleted biomass during cyanobacterial N2-fixation at high Fe concentrations. Journal of Geophysical Research-Biogeosciences 113, G03014, doi:10.1029/2007JG000651.
Zhang, C.L., Horita, J., Cole, D.R., Zhou, J., Lovley, D.R. and Phelps, T.J., 2001. Temperature-dependant oxygen and carbon isotope fractionations of biogenic siderite. Geochimica et Cosmochimica Acta 65, 2257-2271.

Table 1
Stratigraphic unit, depth in the drill core, rock type and mineralogical description of the samples from the Mount McRae Shale and Brockman Iron Formation analyzed in this study.

Stratigraphic unit	Sample #	Depth, m	Rock type	Mineralogy
Brockman Iron Formation				
Joffre Member	J1-124-1	124.7	stilp-rich mudrock	stilp, qtz, K-fdsp, carb (5%), chl, sulfide
Joffre Member	J1-138-1	138.7	calcareous stilp-rich mudrock	stilp, qtz, K-fdsp, carb (30%), chl, sulfide
Joffre Member	J1-148-2	148.2	calcareous stilp-rich mudrock	Fe-carb (37%; siderite), stilp, biot, minor chl, sulfide
Joffre Member	J1-148-3	148.2	stilp-rich mudrock	stilp, sulfide, carb (3%)
Joffre Member	J1-162-1	162	stilp-rich mudrock	stilp, qtz, fdsp, sulfide*
Whaleback Shale	WS188	188	stilp-rich mudrock	stilp, qtz, fdsp, chl, biot, carb (9%)
Whaleback Shale	WS196	196.8	calcareous stilp-rich mudrock	stilp, carb (30%), K-fdsp, qtz, rare biot, sulfide
Dales Gorge Member	DGM236	236.6	calcareous stilp-rich mudrock	stilp, carb (40%), qtz, fdsp, chl, biot, rare sulfide
Dales Gorge Member	DGM243	243	calcareous stilp-rich mudrock	K-fdsp, biot, qtz, stilp, carb (20%), rare sulfide
Dales Gorge Member	DGM258-1	258.3	calcareous stilp-rich mudrock	stilp, carb (25%), Fe-ox, rare biot, sulfide
Dales Gorge Member	DGM258-2	258.3	calcareous stilp-rich mudrock	stilp, carb (45%), Fe-ox, rare biot, sulfide
Dales Gorge Member	DGM268	268.8	calcareous stilp-rich mudrock	stilp, carb (14%), minor qtz, fdsp, sulfide
Dales Gorge Member	DGM271-2	271.8	stilp-rich mudrock	stilp (40%), chl (60%)
Dales Gorge Member	DGM287	287	calcareous stilp-rich mudrock	qtz, K-fdsp, biot, carb (10%), chl, org. mat., sulfide
Dales Gorge Member	DGM288-1	288	calcareous stilp-rich mudrock	stilp, Fe-carb (53%, siderite)
Dales Gorge Member	DGM288-2	288	BIF	chert, carb (83%, siderite)
Dales Gorge Member	DGM302	302.6	calcareous stilp-rich mudrock	Fe-carb (42%), stilp, biot, minor chl, sulfide
Dales Gorge Member	DGM307-4	307.9	BIF	Fe-ox, carb (20%), minor stilp, sulfide
Dales Gorge Member	DGM307-6	307.9	Fe-carb-rich chert	chert, carb (23%, ankerite)
Dales Gorge Member	DGM325	325.6	calcareous stilp-rich mudrock	stilp, chl, biot, carb (20%), sulfide
Dales Gorge Member	DGM337	337.9	calcareous stilp-rich mudrock	stilp, chl, biot, carb (30%, ferroan dolomite), sulfide
Dales Gorge Member	DGM350	350.85	stilp-rich mudrock	stilp, qtz, chl, K-fdsp, carb (10%)
Mount McRae Shale				
Colonial Chert	CC364	364	BIF	Fe-ox, Fe-carb (35%; siderite), minor stilp, chl, sulfide
Colonial Chert	CC367	367.7	calcareous stilp-rich mudrock	stilp, chl, carb (11%), minor fdsp, sulfide
Colonial Chert	CC373	373.9	stilp-rich mudrock	stilp, chl, carb (8%), minor fdsp, sulfide
Colonial Chert	CC376	376.5	stilp-rich mudrock	stilp, chl, carb (3%), minor fdsp
Mc Rae Shale	MR379	379.9	organic-rich marl	carb (40%; dolomite), qtz, K-fdsp, biot, org. mat., sulfide
Mc Rae Shale	MR381	381	organic-rich marl	carb (50%; dolomite), qtz, K-fdsp, biot, org. mat., sulfide
Mc Rae Shale	MR382	382.3	calcareous black shale	qtz, K-fdsp, biot, carb (8%; dolomite), org. mat., sulfide
Mc Rae Shale	MR383	383.8	organic-rich marl	carb (60%; dolomite), qtz, K-fdsp, biot, org. mat., sulfide
Mc Rae Shale	MR387	387.4	organic-rich marl	carb (60%; dolomite), qtz, K-fdsp, biot, org. mat., sulfide

Column 4 includes 4 types of rocks : organic-rich marls, stilpnomelane-rich mudrocks, calcareous (i.e. >10% carb) stilpnomelane-rich mudrocks, banded iron formation (BIF), and one chert rich in Fe-carbonates.
Column 5: mineralogy from thin section and SEM analyses. The values in brackets indicate the proportion of carbonates as determined from H_3PO_4 decarbonation (see details in the analytical section). Abbreviations: stilp: stilpnomelane; qtz: quartz; K-fdsp: potassic feldspar; carb: carbonates; chl: chlorite; biot: biotite; Fe-ox: Fe-oxides (hematite and/or magnetite), org. mat.: high organic matter content; Fe-carb: Fe-rich carbonate.

Table 2
Major element concentrations in samples from the Mount McRae Shale and Brockman Iron Formation (in wt.%).

Sample #	SiO_2	Al_2O_3	Fe_2O_3	MnO	MgO	CaO	Na_2O	K_2O	TiO_2	P_2O_5	LOI	Total
J1-124-1	55.02	12.72	14.51	0.03	2.62	1.14	0.25	11.36	0.08	0.05	2.78	100.55
J1-138-1	30.02	2.99	41.38	0.64	5.67	0.44	0.41	1.47	0.09	0.08	17.11	100.31
J1-148-3	44.14	4.85	35.21	0.12	5.44	0.28	0.70	2.48	0.14	0.07	7.00	100.41
J1-148-2	25.02	2.99	41.98	0.60	6.79	1.28	0.38	1.54	0.07	0.07	19.72	100.44
J1-162-1	45.57	6.72	31.45	0.05	5.85	0.04	0.59	3.90	0.12	0.07	6.19	100.53
WS188	36.29	9.25	31.22	0.16	6.82	1.39	0.27	4.26	0.16	0.31	9.80	99.93
WS196	33.56	7.85	19.78	0.33	6.11	9.41	0.26	5.90	0.34	0.11	15.78	99.44
DGM236	29.59	5.29	28.57	0.53	5.51	6.04	0.18	4.06	0.17	0.13	19.24	99.30
DGM243	46.38	12.46	11.21	0.22	3.66	5.77	0.11	10.48	0.26	0.10	9.98	100.63
DGM258-1	29.37	3.14	43.02	0.47	5.20	0.81	0.27	2.33	0.11	0.09	14.49	99.30
DGM258-2	23.10	2.71	38.85	0.57	5.94	5.68	0.21	2.00	0.14	0.07	19.85	99.11
DGM268	37.66	7.29	26.23	0.36	7.79	4.27	0.67	2.91	0.32	0.13	12.22	99.84
DGM271-2	29.53	15.37	35.16	0.07	11.54	-	0.14	0.51	0.17	0.06	7.67	100.21
DGM287	51.28	12.40	13.24	0.13	5.94	3.04	-	5.60	0.50	0.17	8.37	100.65
DGM288-1	14.01	1.38	45.55	0.73	9.18	1.92	0.23	0.62	0.03	0.18	26.47	100.29
DGM288-2	8.96	0.74	43.81	0.86	10.53	2.40	0.13	0.37	0.01	0.24	31.11	99.16
DGM302	24.53	2.38	45.34	0.29	5.65	1.07	0.45	0.97	0.09	0.11	19.85	100.73
DGM307-4	14.26	1.42	64.78	0.18	3.75	4.20	0.29	0.56	0.03	1.95	9.64	101.06
DGM307-6	73.13	0.19	6.71	0.11	2.32	6.86	-	0.05	0.00	-	10.53	99.90
DGM325	33.24	4.38	37.21	0.37	5.87	2.18	0.76	1.67	0.21	0.09	14.11	100.08
DGM337	29.06	6.63	26.82	0.12	8.95	8.80	0.69	1.09	0.29	0.08	17.90	100.43
DGM350	49.65	3.43	25.88	0.13	7.32	0.67	0.65	1.29	0.01	0.07	9.97	99.05
CC364	4.56	0.18	78.16	0.13	3.12	3.19	-	0.12	0.01	0.17	10.54	100.19
CC367	34.64	7.77	29.92	0.08	10.09	3.09	0.53	1.07	0.28	0.11	12.13	99.70
CC373	37.77	6.68	31.94	0.05	9.34	0.65	0.71	1.38	0.24	0.08	10.34	99.18
CC376	38.67	7.90	30.37	0.04	10.77	0.63	0.64	1.37	0.29	0.09	8.71	99.48
MR379	35.82	9.58	6.19	0.28	8.33	13.15	-	4.98	0.33	0.06	21.31	100.03
MR381	31.89	7.71	4.60	0.38	8.44	16.53	-	4.51	0.27	0.05	24.94	99.34
MR382	59.32	14.03	2.31	0.07	2.94	2.35	0.21	9.34	0.46	0.07	8.75	99.85
MR383	29.01	8.71	2.71	0.39	10.37	16.77	0.11	6.03	0.12	0.03	26.32	100.55
MR387	27.90	7.55	3.28	0.28	10.18	17.55	-	3.91	0.23	0.04	29.21	100.13

Table 3
Carbonate and organic carbon contents and their C isotopic compositions, bulk N content and its isotopic composition, C/N and Fe/Ti molar ratios in samples from the Mount McRae Shale and Brockman Iron Formation

Sample #	$C_{carb\ 80°C}$, wt%	$C_{carb\ 130°C}$, wt%	$C_{carb\ total}$, wt%	$\delta^{13}C_{carb\ total}$, ‰	C_{org}, wt%	$\delta^{13}C_{org}$, ‰	N_{bulk}, ppm	$\delta^{15}N$, ‰	C_{org}/N_{bulk}	Fe/Ti
J1-124-1	4.4	bdl	4.4	-8.6	0.14	-28.27	87.4	9.5	18.9	188.4
J1-138-1	11.7	21.3	33.1	-8.6	0.41	-28.70	16.7	8.1	285.9	465.0
J1-148-3	1.5	1.7	3.2	-7.9	0.52	-28.64	46.5	9.5	129.9	258.9
J1-148-2	12.4	24.5	36.9	-8.3	0.35	-28.22	40.3	8.6	102.5	617.4
J1-162-1	0.1	bdl	0.1	bdl	0.28	-28.74	121.3	7.4	26.7	273.5
WS188	4.6	3.9	8.5	-7.8	0.66	-28.98	8.6	5.1	894.6	200.1
WS196	32.5	bdl	32.5	-5.1	0.42	-27.62	173.3	6.0	28.4	58.4
DGM236	25.2	14.7	39.9	-8.1	0.70	-28.34	54.0	9.0	150.4	167.1
DGM243	17.9	bdl	17.9	-9.3	0.93	-29.04	100.0	9.2	108.8	43.6
DGM258-1	11.6	15.0	26.6	-7.4	0.49	-28.48	63.2	13.4	90.5	384.1
DGM258-2	29.8	16.2	46.0	-7.2	1.06	-28.61	62.8	11.6	196.2	285.7
DGM268	13.3	1.0	14.3	-5.5	1.39	-29.24	113.9	4.2	142.7	81.5
DGM271-2	0.1	bdl	0.1	bdl	0.67	-28.62	31.2	7.6	250.6	204.4
DGM287	9.7	bdl	9.7	-6.1	1.93	-31.29	186.1	4.8	120.9	26.5
DGM288-1	21.5	31.7	53.1	-7.0	1.44	-29.95	40.6	0.4	415.0	1469.3
DGM288-2	-	83.3	83.3	-6.8	1.20	-28.92	6.2	5.8	2250.9	5475.9
DGM302	24.7	18.2	42.9	-8.0	0.28	-28.70	6.0	6.3	547.3	487.5
DGM307-4	14.7	6.7	21.3	-7.9	0.18	-28.29	6.0	8.0	348.4	2491.4
DGM307-6	22.7	bdl	22.7	-7.8	0.05	-26.43	1.3	7.9	421.4	1678.0
DGM325	11.8	11.3	23.1	-9.0	0.29	-28.76	24.2	8.8	138.7	179.8
DGM337	29.6	2.0	31.6	-9.2	0.41	-28.41	10.7	9.9	443.5	94.1
DGM350	4.4	5.8	10.1	-10.7	0.22	-29.22	7.6	11.1	345.1	2876.0
CC364	20.4	15.2	35.6	-9.2	0.59	-28.16	83.9	6.7	81.5	7816.4
CC367	9.1	1.2	10.3	-5.9	1.22	-28.48	38.8	3.2	367.4	105.4
CC373	3.7	4.6	8.3	-9.2	0.70	-28.85	30.4	7.0	267.0	133.1
CC376	1.7	1.2	2.9	-10.5	0.62	-28.63	61.7	6.9	117.8	104.7
MR379	40.0	bdl	40.0	-4.2	1.74	-28.83	384.7	5.4	52.8	18.5
MR381	51.1	bdl	51.1	-3.9	2.64	-28.59	385.5	5.7	80.0	16.9
MR382	8.0	bdl	8.0	-3.7	3.05	-29.39	785.5	4.4	45.2	5.1
MR383	56.0	bdl	56.0	-3.2	1.92	-29.15	497.5	4.4	45.0	23.5
MR387	57.9	bdl	57.9	-5.6	4.58	-30.48	420.1	4.6	127.2	14.2

bdl: bellow detection limit.
C_{org}/N_{bulk} and Fe/Ti are molar ratios.

Figure captions

Fig. 1. Geological map of the Hamersley Province and stratigraphic divisions of the upper part of the Hamersley Group showing the location of the drill-core WLT-10 and stratigraphic position of the geological units discussed in this work (modified from Krapež et al., 2003). The boundary between the Chichester Range and Hamersley Range megasequences is the unconformity at the base of the Mount Sylvia Formation (Blake and Barley, 1992).

Fig. 2. Major element concentrations (in wt%) of the samples analyzed in our study, including organic-rich shales from the Mount McRae Shale, and stilpnomelane-rich mudrocks, banded iron formations and chert from the Brockman Iron Formation. Samples are marked as "calcareous" if their total carbonate content is higher than 10 wt%.

Fig. 3. Organic carbon content (in wt%) and whole-rock nitrogen content (in ppm) versus Fe/Ti molar ratio in samples from the Mount McRae Shale (organic-rich shales) and Brockman Iron Formation (all other lithologies). Low Fe/Ti molar ratio indicates a predominantly detrital Fe flux, while high Fe/Ti molar ratio points to a higher flux of authigenic Fe.

Fig. 4. Variations in organic C and whole-rock N contents and isotopic compositions, and C isotope values of whole-rock carbonate as a function of the depth in the drill-core for samples from the Mount McRae Shale (organic-rich shales) and Brockman Iron Formation (all other lithologies). Data of Garvin et al. (2009) for the Mount McRae Shale are also plotted for comparison. See the main text for further discussion. Since samples of Garvin et al. (2009) were collected from other drill-core (ABDP-9) at a different location in the Hamersley Province (21°59'29.5"S, 117°25'13.6"E), the depths reported in their paper were adjusted (shifted down by 275 m) in order to obtain a continuous profile of C and N contents and $\delta^{13}C_{org}$ and $\delta^{15}N$ values.

Fig. 5. Organic C content versus C isotope composition of carbonates in samples from the Mount McRae Shale (organic-rich shales) and Brockman Iron Formation (all other lithologies). A positive trend (albeit with large deviations) suggests that organic matter mineralization was associated with precipitation of secondary carbonates during diagenesis.

Fig. 6. Nitrogen content as a function of organic carbon content (A) and whole-rock potassium content (B) in samples from the Mount McRae Shale (organic-rich shales) and Brockman Iron Formation (all other lithologies). (C) C/N molar ratio versus whole-rock potassium content. Positive correlation in (A) suggests that N was derived from organic matter and in (B) that N was at least partially in form of NH_4^+ substituting for K^+ in stilpnomelane. Decrease in C/N molar ratio with increasing K_2O content indicates that NH_4^+, released from organic matter via mineralization, was partially trapped in stilpnomelane.

Fig. 7. Nitrogen isotope composition versus C_{org}/N molar ratio (A), N concentration (B), and C isotope values of carbonate (C) in samples from the Mount McRae Shale (organic-rich shales) and Brockman Iron Formation (all other lithologies). Decoupling among these parameters suggests that N loss related to diagenesis did not induce any systematic N isotope shift, supporting preservation of primary $\delta^{15}N$ values.

Fig. 8. Schematic models illustrating N biogeochemical cycle in (A) anoxic water column with local O_2 production (noted as "oxygen oases"), (B) fully anoxic water column, and (C) redox-stratified water column. In these models, high productivity is restricted to proximal facies due to a higher nutrient supply as recorded by organic-rich shales of the Mount McRae Shale, while lower productivity is typical for distal environments as represented by the Brockman Iron Formation. High productivity in the Mount McRae Shale depositional environment likely limited NH_4^+ and NO_3^- availability for biological assimilation, thus inducing larger contribution of N_2-fixing bacteria to the biomass resulting in lower $\delta^{15}N$ values. Co-variation of $\delta^{15}N$ and $\delta^{13}C_{carb}$ values in the Brockman Iron Formation (Fig. 4) requires a connection between N and Fe biogeochemical cycles in the water column (see the main text for further details). Under anoxic conditions (models A and B), the dominant N species available for biological assimilation in the photic zone would be NH_4^+. Positive $\delta^{15}N$ values under these conditions may reflect partial consumption of NH_4^+ by O_2-driven nitrification (A) or microbial oxidation utilizing Fe(III) oxyhydroxides (B) formed in the water column. Under redox-stratified conditions (model C), N in the form of NO_3^- would be assimilated by primary producers. Highly positive $\delta^{15}N$ values would be expected under

high denitrification conditions, related to high rates of microbial Fe(II) oxidation at the redox boundary.

Figure 1

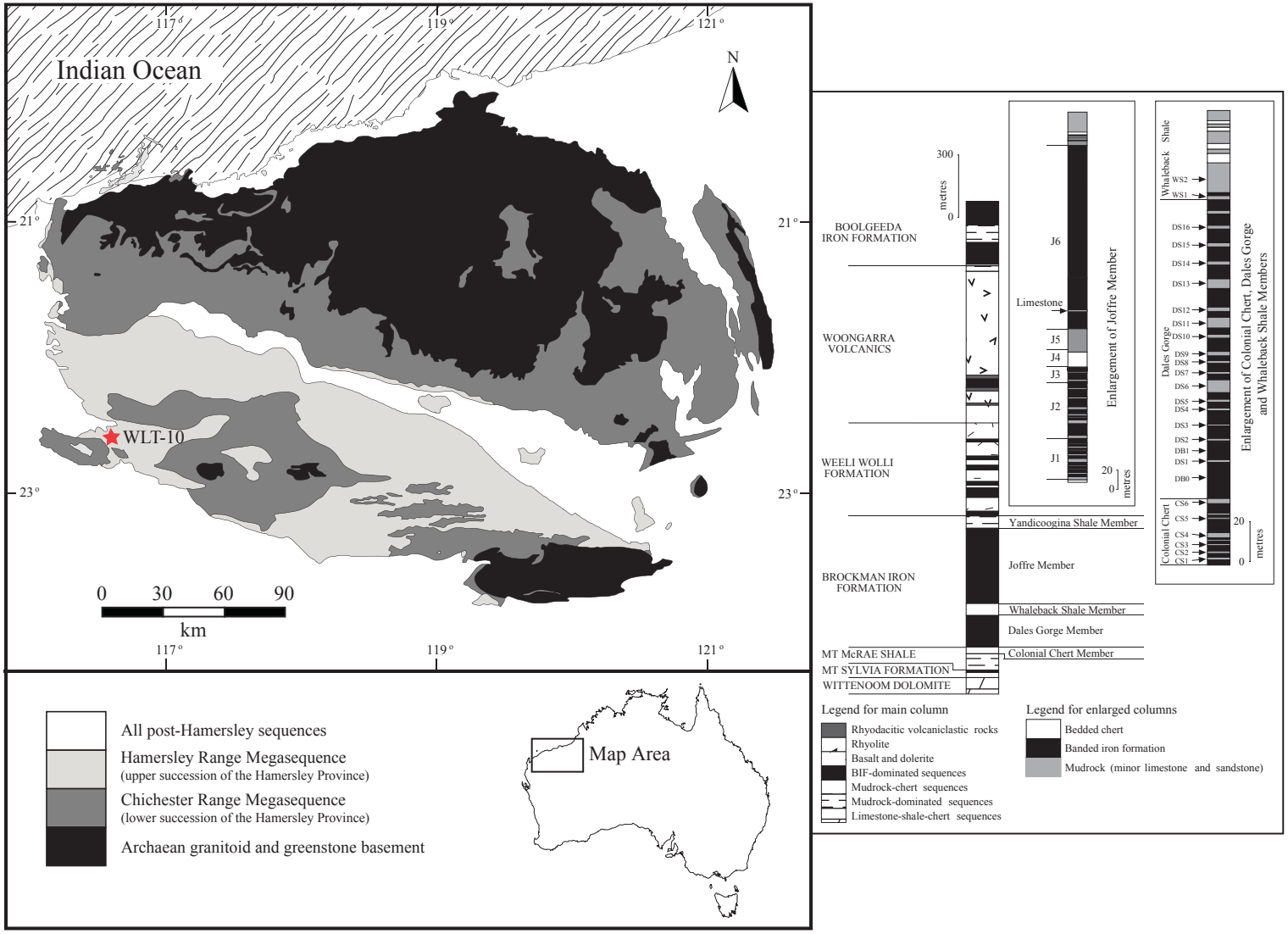
Indian Ocean
N
117°
119°
121°
21°
23°
WLT-10
0 30 60 90
km
All post-Hamersley sequences
Hamersley Range Megasequence
(upper succession of the Hamersley Province)
Chichester Range Megasequence
(lower succession of the Hamersley Province)
Archaean granitoid and greenstone basement
Map Area
300
metres
0
BOOLGEEDA IRON FORMATION
WOONGARRA VOLCANICS
WEELI WOLLI FORMATION
BROCKMAN IRON FORMATION
MT McRAE SHALE
MT SYLVIA FORMATION
WITTENOOM DOLOMITE
Yandicoogina Shale Member
Joffre Member
Whaleback Shale Member
Dales Gorge Member
Colonial Chert Member
J6
Limestone
J5
J4
J3
J2
J1
Enlargement of Joffre Member
20
0
metres
Whaleback Shale
WS2
WS1
DS16
DS15
DS14
DS13
DS12
DS11
DS10
DS9
DS8
DS7
DS6
DS5
DS4
DS3
DS2
DB1
DS1
DB0
Dales Gorge
CS6
CS5
CS4
CS3
CS2
CS1
Colonial Chert
Enlargement of Colonial Chert, Dales Gorge and Whaleback Shale Members
Legend for main column
Rhyodacitic volcaniclastic rocks
Rhyolite
Basalt and dolerite
BIF-dominated sequences
Mudrock-chert sequences
Mudrock-dominated sequences
Limestone-shale-chert sequences
Legend for enlarged columns
Bedded chert
Banded iron formation
Mudrock (minor limestone and sandstone)

Figure 2

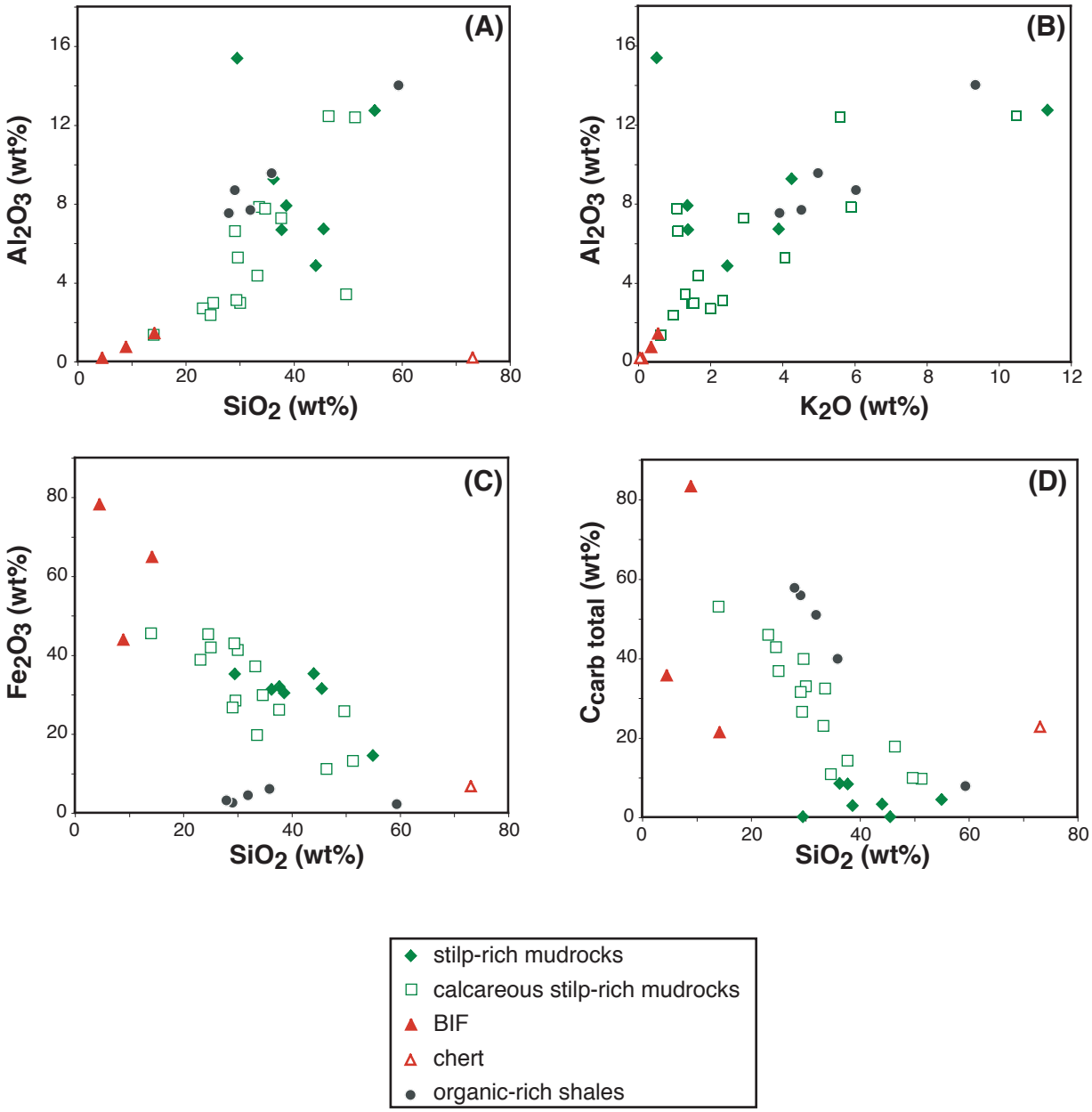
(A)
Al2O3 (wt%)
SiO2 (wt%)
(B)
Al2O3 (wt%)
K2O (wt%)
(C)
Fe2O3 (wt%)
SiO2 (wt%)
(D)
Ccarb total (wt%)
SiO2 (wt%)
stilp-rich mudrocks
calcareous stilp-rich mudrocks
BIF
chert
organic-rich shales

Figure 3

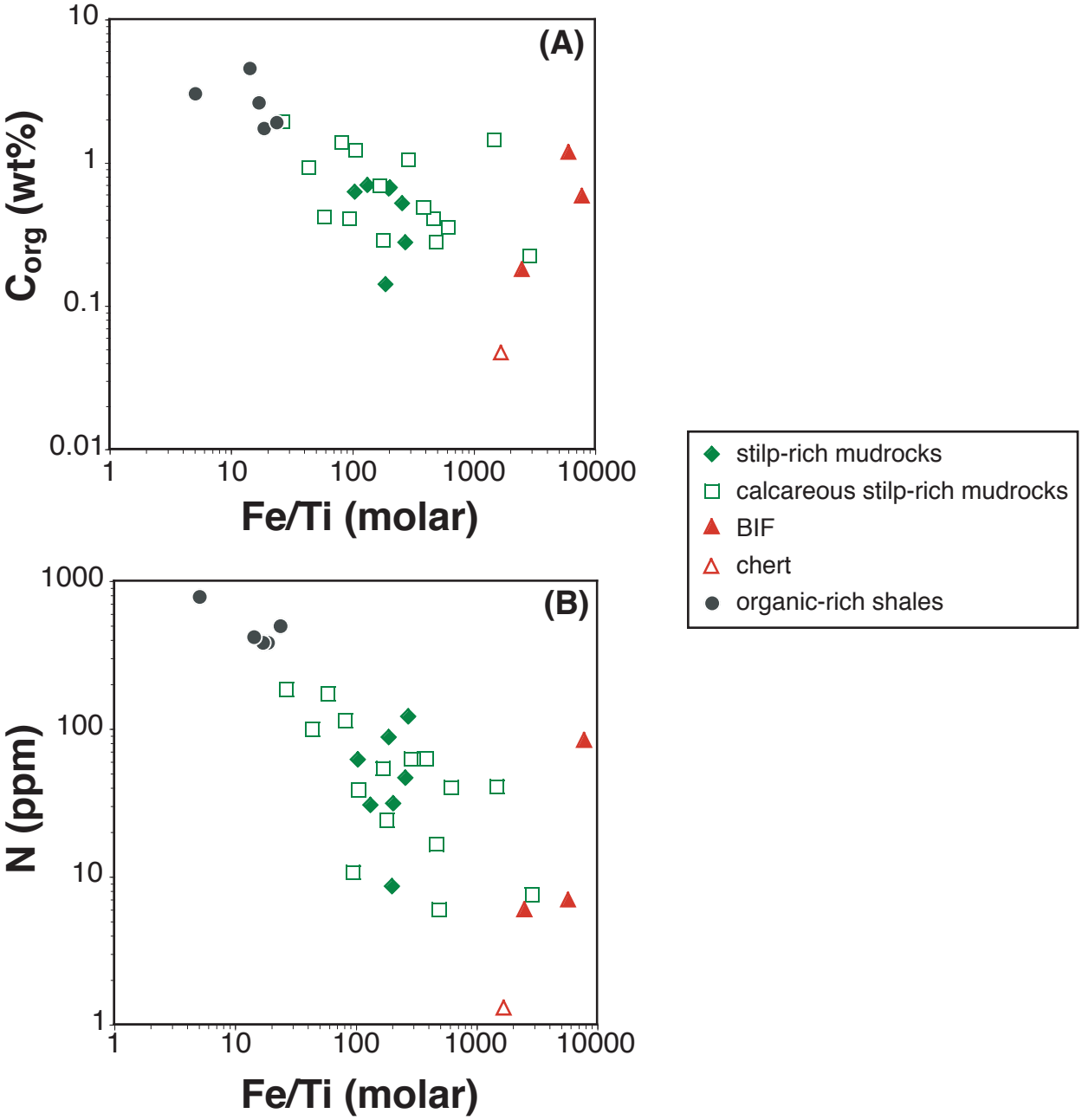
(A)
C_{org} (wt%)
10
1
0.1
0.01
1
10
100
1000
10000
Fe/Ti (molar)
(B)
N (ppm)
1000
100
10
1
1
10
100
1000
10000
Fe/Ti (molar)
stilp-rich mudrocks
calcareous stilp-rich mudrocks
BIF
chert
organic-rich shales

Figure 4

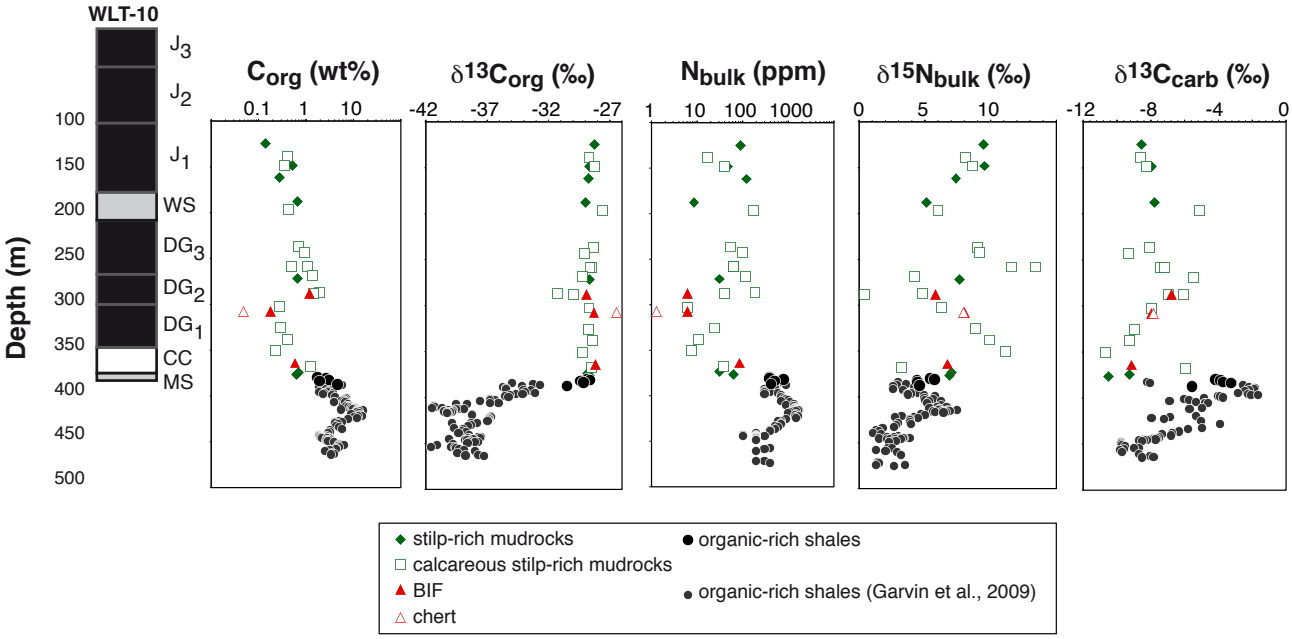
WLT-10
Depth (m)
100
150
200
250
300
350
400
450
500
J3
J2
J1
WS
DG3
DG2
DG1
CC
MS
Corg (wt%)
0.1
1
10
δ13Corg (‰)
-42
-37
-32
-27
Nbulk (ppm)
1
10
100
1000
δ15Nbulk (‰)
0
5
10
δ13Ccarb (‰)
-12
-8
-4
0
stilp-rich mudrocks
calcareous stilp-rich mudrocks
BIF
chert
organic-rich shales
organic-rich shales (Garvin et al., 2009)

Figure 5

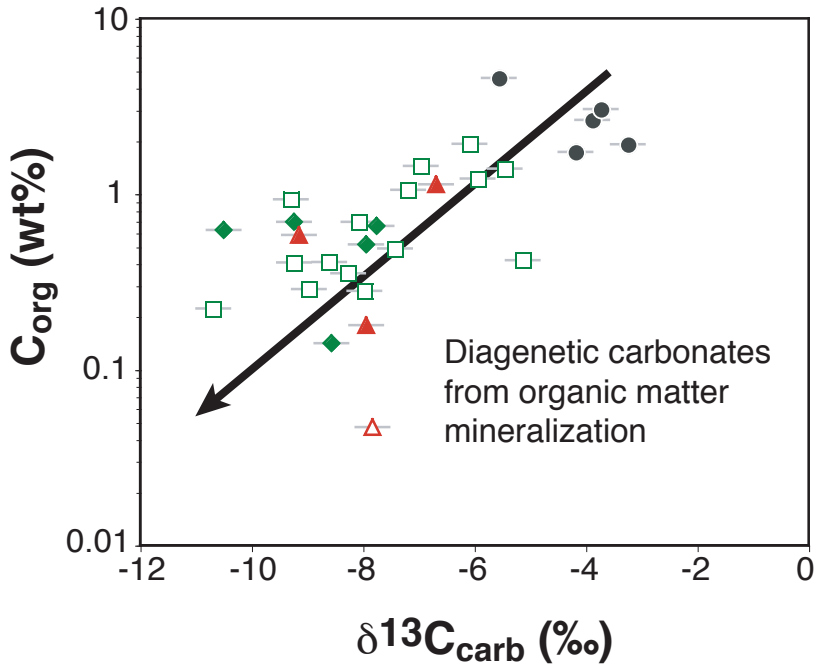
10
1
0.1
0.01
-12
-10
-8
-6
-4
-2
0
C_{org} (wt%)
$\delta^{13}C_{carb}$ (‰)
Diagenetic carbonates
from organic matter
mineralization

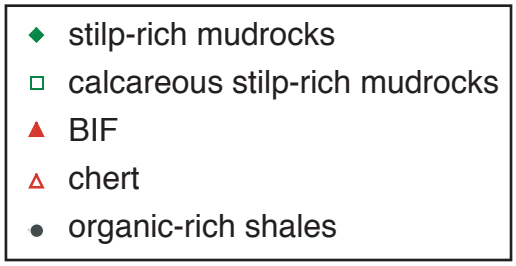
stilp-rich mudrocks
calcareous stilp-rich mudrocks
BIF
chert
organic-rich shales

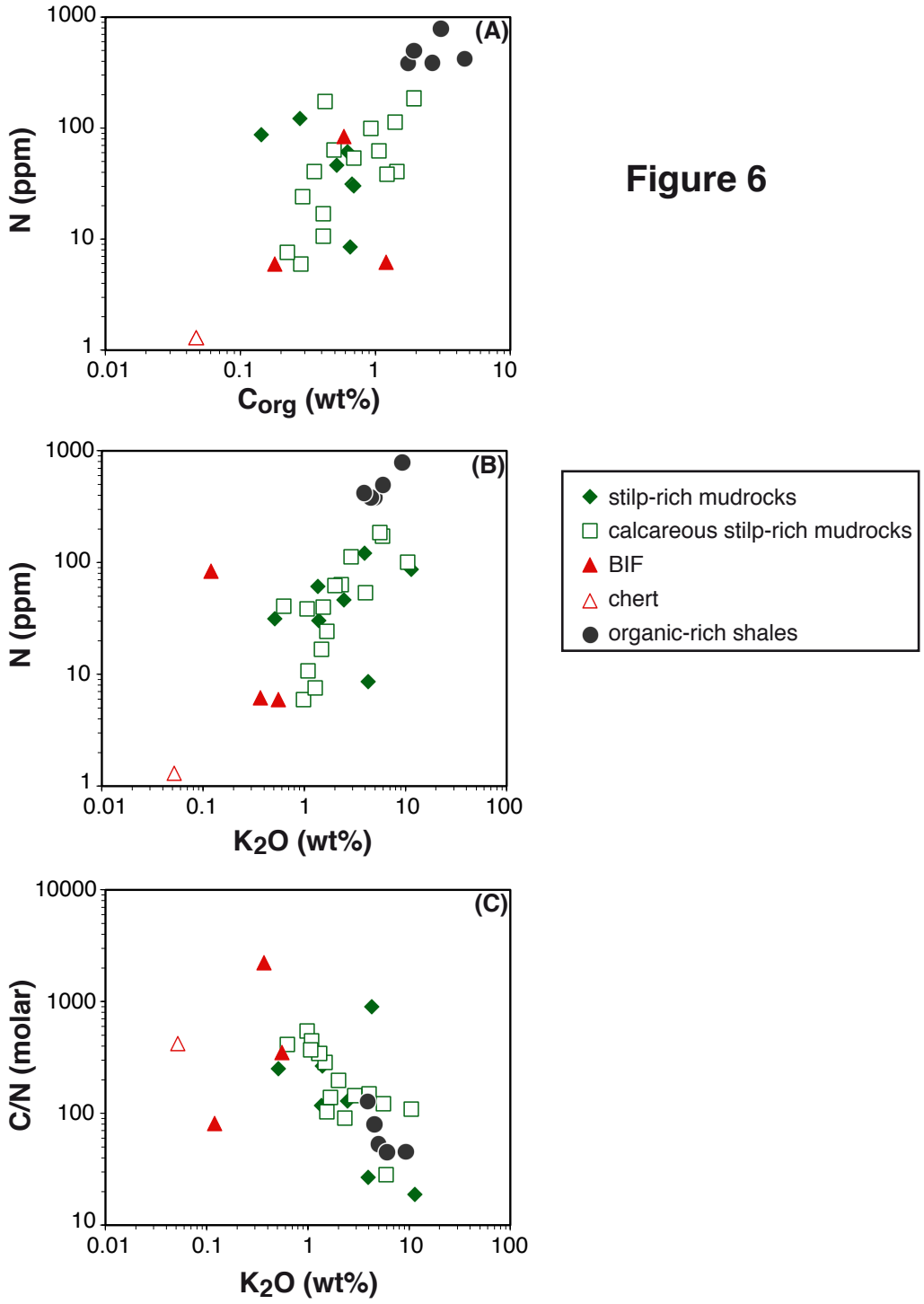
(A)
N (ppm)
1000
100
10
1
0.01
0.1
1
10
Corg (wt%)
(B)
N (ppm)
1000
100
10
1
0.01
0.1
1
10
100
K2O (wt%)
(C)
C/N (molar)
10000
1000
100
10
0.01
0.1
1
10
100
K2O (wt%)
stilp-rich mudrocks
calcareous stilp-rich mudrocks
BIF
chert
organic-rich shales

Figure 6

Figure 7

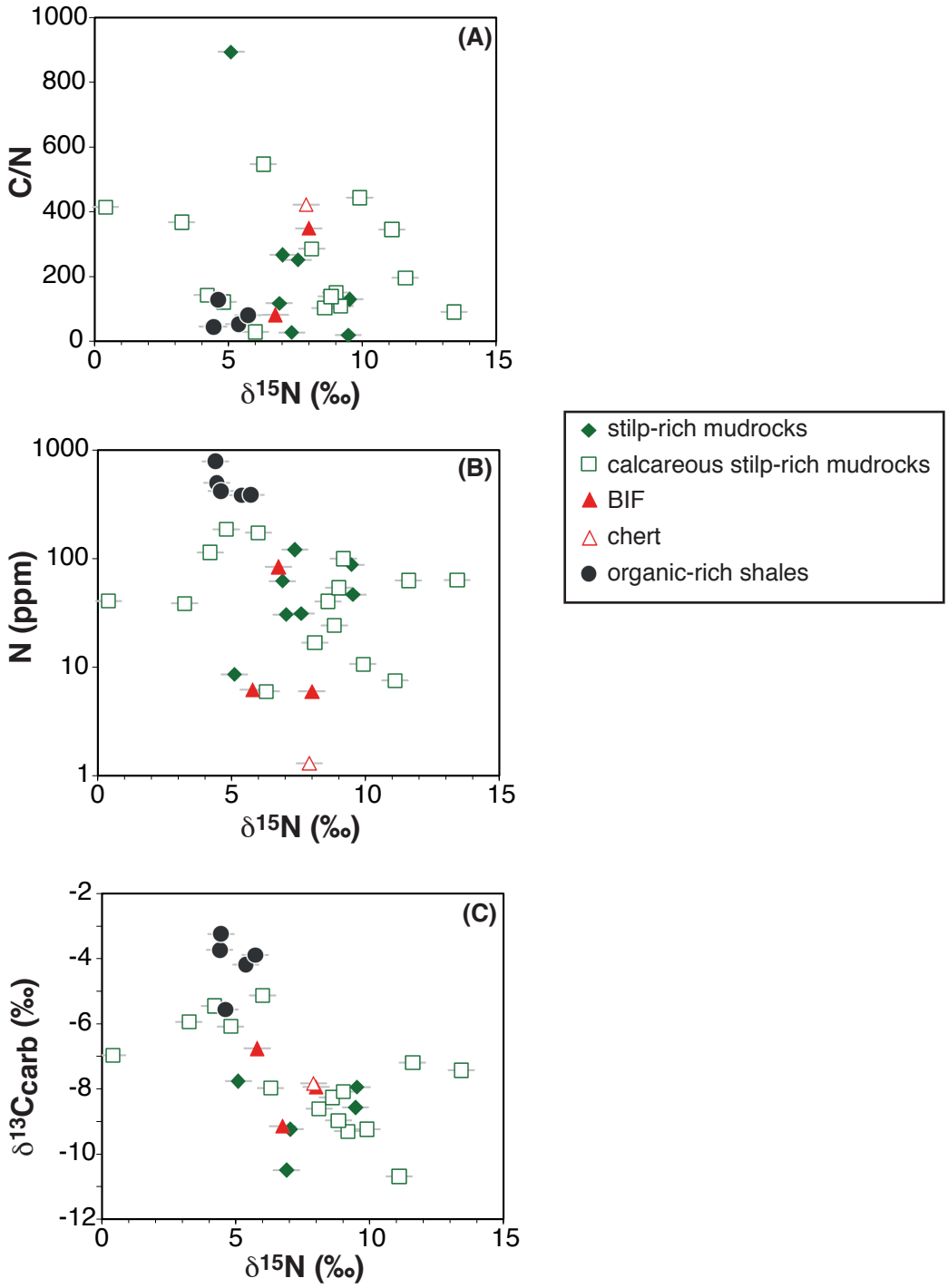
(A)
C/N
1000
800
600
400
200
0
0
5
10
15
δ15N (‰)
(B)
N (ppm)
1000
100
10
1
0
5
10
15
δ15N (‰)
(C)
δ13Ccarb (‰)
-2
-4
-6
-8
-10
-12
0
5
10
15
δ15N (‰)
stilp-rich mudrocks
calcareous stilp-rich mudrocks
BIF
chert
organic-rich shales

Figure 8

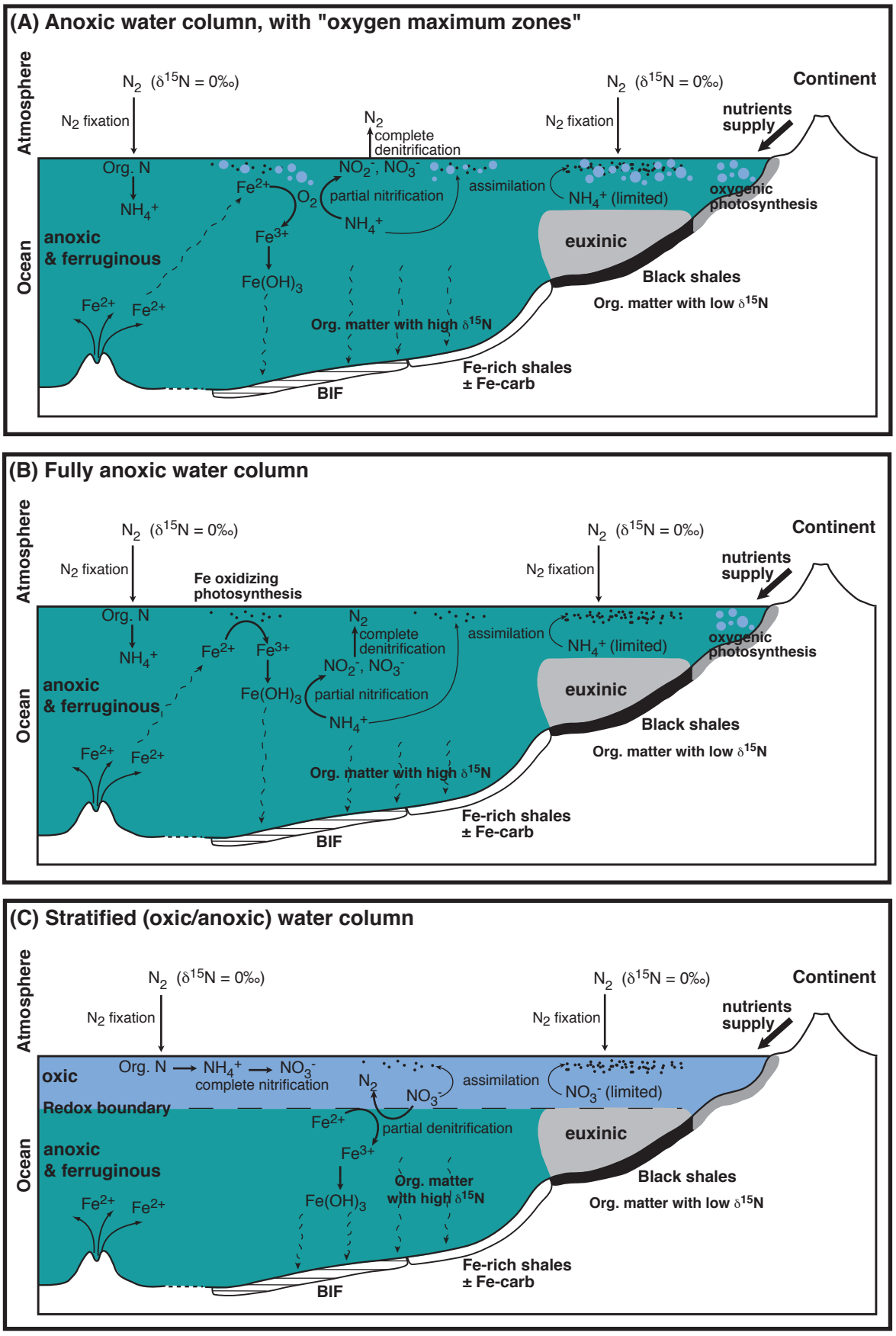
(A) Anoxic water column, with "oxygen maximum zones"
Atmosphere
Ocean
N2 (δ15N = 0‰)
N2 fixation
N2
complete denitrification
Continent
nutrients supply
Org. N
NH4+
Fe2+
O2
partial nitrification
NO2-, NO3-
assimilation
NH4+ (limited)
oxygenic photosynthesis
anoxic & ferruginous
Fe3+
Fe(OH)3
euxinic
Black shales
Org. matter with low δ15N
Org. matter with high δ15N
Fe-rich shales ± Fe-carb
BIF
(B) Fully anoxic water column
Fe oxidizing photosynthesis
(C) Stratified (oxic/anoxic) water column
oxic
Redox boundary
Org. N → NH4+ → NO3-
complete nitrification
NO3- (limited)
partial denitrification
Org. matter with high δ15N
Brockman Iron Formation
- low nutrients
- low productivity
- high δ15N
Mount Mc Rae Shale
- high nutrients
- high productivity
- low δ15N